Chirality Transfer from Subnanometer Biochemical Molecules to Submicrometer Plasmonic Metastructures: Physiochemical Mechanisms, Biosensing and Bioimaging Opportunities

*Zhaolong Cao, Han Gao, Meng Qiu, Wei Jin, Shaozhi Deng, Kwok-yin Wong, Dangyuan Lei**

Dr. Z. L. Cao, Prof. S. Z. Deng
State Key Laboratory of Optoelectronic Materials and Technologies, Guangdong Province Key Laboratory of Display Material and Technology, School of Electronics and Information Technology, Sun Yat-sen University, Guangzhou 510275, China.

H. Gao, Dr. M. Qiu, Prof. W. Jin
Department of Electrical Engineering
The Hong Kong Polytechnic University
Hong Kong 999077, China

Prof. K.-Y. Wong
Department of Applied Biology and Chemical Technology
The Hong Kong Polytechnic University
Hong Kong 999077, China

Dr. D. Y. Lei
Department of Materials Science and Engineering
City University of Hong Kong
Hong Kong 999077, China
E-mail: dangylei@cityu.edu.hk

Keywords: optical chirality, chirality transfer, plasmon resonance, circular dichroism

Abstract:

Determining the structural chirality of biomolecules is of vital importance in bioscience and biomedicine. Conventional methods for characterizing molecular chirality, e.g. circular dichroism (CD) spectroscopy, require high-concentration specimens due to the weak electronic CD signals of biomolecules such as amino acids. Artificially designed chiral plasmonic metastructures exhibit strong intrinsic chirality. However, the significant size mismatch between metastructures and biomolecules makes the former unsuitable for chirality recognition-based molecular discrimination. Fortunately, constructing metallic architectures through molecular self-assembly allows chirality transfer from subnanometer biomolecules to submicrometer intrinsically-achiral plasmonic metastructures by means of either near-field interaction or chirality inheritance, resulting in hybrid systems with CD signals orders of magnitude larger than that of pristine biomolecules. This exotic property provides a new means to determine molecular chirality at extremely low concentrations (ideally at the single-molecule level). In this review, three strategies of chirality transfer from subnanometer biomolecules to submicrometer metallic metastructures are analysed.

It elaborates the physiochemical mechanisms responsible for chirality transfer, outlines new fascinating opportunities for employing plasmonic metastructures in the trace-level detection of chiral biomolecules and metal ions, and also in chirality-based biosensing and bioimaging.

1. Introduction

A chiral object refers to a geometrical object, or a group of points, whose mirror image cannot be bought to coincide with itself.[1] Most generally, chirality is understood as a lack of mirror symmetry, and achirality means the existence of mirror symmetry. Although the beauty of mirror symmetry has been appreciated for millenaries in ancient arts such as Egyptian pyramids, Mesopotamian mosaics and ancient Chinese architecture etc., less attention has been paid to chiral objects. In fact, chirality is ubiquitous in nature, ranging from macroscopic systems such as human hands to molecular systems like carbohydrates. In 1848, Louis Pasteur achieved the first resolution of racemic acid, demonstrating the existence of chiral molecules.[2] Through this meticulous experiment, the molecule dissymmetry was proved to be the cause of optical activity (OA).[2] His work laid the foundation of what we now call stereochemistry, which has been an important sub-discipline of chemistry.[3] Since then, scientists have endeavored to study and manipulate the spatial arrangement of atoms that form the structure of chiral molecules.

A chiral object and its mirror image are called enantiomorphs or enantiomers, with one labeled as "left-handed" and the other labeled as "right-handed". Interestingly, most chiral biomolecules manifest themselves only in one handedness. For example, the 21 essential amino acids are all L-enantiomers. This phenomenon, called "homochirality", indicates that physiological processes show distinct stereoselectivity although exceptions exist.[4] In pharmacy, statistics shown that about more than a half of the drugs currently applied are chiral compounds,[5, 6] and drugs such as ketamine, penicillamine, and ethambutol can perform correct pharmacological actions only with specific handedness, whereas a 'wrongly-handed' version may be toxic.[7-9] Since molecular chirality lies at the heart of chemical, biological, and physiological processes, sensing and discriminating enantiomers is thus of particular importance in pharmaceutical industry, toxicology, and stereochemistry.

Although crucial, chirality is a subtle property to detect or manipulate at the first glance, as biochemical molecules typically can be found on the length scale of nanometers and even below. A large number of analytical methods, including liquid-phase separation,[10] mass spectrometric techniques,[11] gas chromatography,[12] capillary electrophoresis,[13] and nuclear magnetic resonance protocols[14] have been used for enantiomer discrimination.[11, 15] However, most of these conventional techniques suffer from unavoidable disadvantages such as complex experimental setup, long-time sample pretreatment, expensive chiral stationary phases or chiral selectors. Fortunately, the chirality of biomolecules can manifest itself optically, which has made optical spectroscopic measurements of molecular chiral-optical (chiroptical) effects attractive as they provide label-free, non-invasive and cost-efficient characterizations.[16-22] Chiroptical effects often refer to those phenomena that chiral structures respond differently to the dissymmetric electromagnetic fields. From a

classical point of view, chiroptical effects originate from the fact that enantiomers exhibit distinct refractive indices and extinction coefficients for left- (LCP) and right-circularly polarized (RCP) lights.[23] The former results in optical rotatory dispersion (ORD), that is, rotation of the plane of a linearly polarized light when traveling through a chiral medium, whereas the difference in extinction coefficients causes CD. CD is usually measured as the differential absorption of LCP and RCP lights by chiral molecules. Similar to the real and imaginary part of the refractive index for an achiral medium, CD and ORD are Kramers–Kronig related and it is thus possible to obtain ORD from CD spectrum.[23]

ORD and CD spectroscopies have been widely employed in chemistry, biology, pharmacy as well as physics.[24, 25] They usually require the use of high-concentration specimens because the chiroptical response of natural molecules is extremely weak and often located in the ultraviolet (UV) band. The UV response results from the electronic structure of molecules, and the weak chiroptical signal is largely due to the difference in dimension between UV light and molecules. Surface plasmons, collective electron density oscillations at dielectric/metal interfaces,[26-30] can dramatically enhance chiroptical responses by concentrating far-field electromagnetic waves into subwavelength volumes. Over the past decade, many studies have demonstrated the feasibility of transferring molecular chirality to plasmonic nanostructures,[16, 18, 19, 31, 32], opening up a plethora of possibilities for chiral biosensing and bioimaging down to the single-molecule regime. A primary driving force behind this development is the breakthrough in design and fabrication of artificial metallic nanostructures, ranging from top-down techniques such as focused ion beam milling,[33] electron-beam lithography[34] and direct laser writing,[35] to bottom-up methods like chemical synthesis and self-assembly[32, 36]. Together with theories that can elegantly describe the interaction between chiral molecules and plasmonic nanostructures,[37-40] the study of chirality has entered a fast development path. There have been several reviews focusing on various aspects of this field, including fabrication,[32, 36, 41, 42] theories,[43-45] and applications.[31, 46, 47] The goal of the present review, as illustrated in Scheme 1, is to elaborate the three physiochemical mechanisms of chirality transfer from subnanometer biochemical molecules to submicrometer metallic nanostructures, namely electromagnetic interaction induced chirality transfer, chiral assembly and chirality inheritance, molecular conformation change induced chirality. Section2 summarizes the prevailing theoretical models for describing the electromagnetic interaction between metallic nanostructures and chiral molecules in terms of different types of plasmonic fields. Section 3 introduces biomolecule-guided chiral assembly and growth of metal nanostructures. Section 4 presents the third mechanism of chirality transfer, that is, the conformation change induced new CD responses in biomolecule-adsorbed metal nanostructures. Chiral plasmonic metastructures-based biochemical sensing and bioimaging applications are given in Section 5, followed with an outlook on the future development of the chirality transfer phenomena in Section 6.

2. Chirality transfer via electromagnetic interaction

2.1 Theoretical background

Research on the electromagnetic interaction between chiral biomolecules and metallic

nanostructures dates back to the 2000s when Schaaff and Whetten et al. discovered the chiroptical activity in gold cluster compounds capped with chiral thiols, i.e., gold cores (smaller than 1 nm) stabilized with glutathione (GSH) adsorbate layers.[48, 49] Subsequent theoretical studies showed that structural distortion of the two-shell metallic core of chiral-ligand-protected metallic nanoclusters induced the nonzero CD spectra.[50, 51] Later on, scientists shifted their interests to chiroptical activity of plasmonic nanocrystals (NCs) decorated with chiral molecules because these systems exhibit CD signals in the plasmon resonance bands.[52] When a chiral molecule is placed in the vicinity of a metallic NC, new CD resonances at the NC plasmon bands can be formed due to the Coulomb dipole-dipole interaction that occurs via the following two mechanisms: (1) the metal NC enhances the electromagnetic field strength at the molecule location, leading to a stronger molecular dipole moment and thus giving rise to an increased CD signal at the molecular electronic CD band; (2) the Coulomb interaction with the excited chiral molecule also induces local chiral currents on the NC surface, resulting in giant differential absorption at the plasmon resonance bands. It is worthwhile noting that, most biomolecules typically have strong CD bands in the UV spectral range, whereas achiral metallic nanostructures exhibit pronounced plasmon resonances in the visible region but without chiroptical activity. Therefore, the direct plasmonic enhancement at the molecular CD bands (Mechanism 1) is usually very weak. Nevertheless, the second mechanism can render the chirality transfer from chiral biomolecules to achiral metallic NCs, giving rise to enhanced CD signals at plasmon resonance bands.

The physical scenario of electromagnetic interaction between a chiral molecule and a metal NC appears complicated because the electric and magnetic fields in the hybrid system are coupled.[53] With the help of theoretical derivations and numerical simulations (e.g., finite element method, finite-difference time-domain method, etc.), one can accurately calculate the electromagnetic response of metallic NCs. However, how to model chiral molecules has been a great challenge in many theoretical studies, among which two approaches are found to show good agreement with experimental observations.[37-40, 54] The first approach was proposed by Govorov *et al*. based on the density-matrix formalism, where a chiral molecule is treated as a two-level system with non-orthogonal magnetic and electric dipole moments and subsequently the CD spectrum of the hybrid molecule-NC complex can be rigorously calculated as the total contribution from the molecule and the NC.[37, 38] In the second approach, Zhang *et al.* simply considered the plasmonic absorption as the dominant contribution to the overall CD of the hybrid system, where the chiral molecule is regarded as an electric dipole with different effective polarizabilities for LCP and RCP excitation.[39, 40] As discussed below, this method represents a classical point of view of isotropic chiral medium, and can be derived from Govorov's quantum treatment by considering Fedorov[55] and Rosenfeld's equations.[56]

2.1.1 Density-matrix formalism

In the density-matrix formalism, a chiral molecule is treated as a two-level system with non-orthogonal electric and magnetic dipole moments. According to the quantum theory of optical activity, the chiroptical response of the chiral molecule is written as:[24, 56]

$$\mathrm{CD}_{\mathrm{molecule}} \propto \mathrm{Im}[\boldsymbol{\mu}_{12} \cdot \boldsymbol{m}_{21}] \quad (1)$$

where $\boldsymbol{\mu}_{12}$ and $\boldsymbol{m}_{21}$ are the electric and magnetic dipole moments of the molecule, and indices 1 and 2 correspond to the molecule's ground and excited states. As depicted in **Figure 1**a, the molecule is placed at a distance Δ from the surface of a plasmonic NC, with a center-to-center distance denoted as $\boldsymbol{R}$. In this formalism, the molecule-NC separation is small enough (a few nanometers) such that the Coulomb dipole-dipole interaction takes effect. The equation of motion of the density matrix used to describe the quantum states of the molecule is expressed as:[37, 38]

$$\hbar \frac{\partial \rho_{nm}}{\partial t} = i\langle n \left| [\hat{\rho}, \widehat{H}_0 + \widehat{\mathbb{V}}] \right| m\rangle - \left(\hat{\Gamma} \cdot \rho\right)_{nm} \quad (2)$$

where $|n\rangle$ and $|m\rangle$ represent two quantum states with $n, m = 1, 2$, $\hat{\Gamma} \cdot \rho$ denotes the relaxation matrix, and the Hamiltonian $\widehat{H}_0 + \widehat{\mathbb{V}}$ includes the internal energy of the molecule and the light-matter interaction.[37] The total absorption of the system can be split into two parts, namely, (1) dissipation inside the molecule due to the enhanced dipole moment and (2) chiral dissipative currents inside the NC induced by the molecule. The total CD signal of the hybrid system can thus be written as:[37, 38]

$$\mathrm{CD}_{\mathrm{total}} = \mathrm{CD}_{\mathrm{molecule}} + \mathrm{CD}_{\mathrm{NC}} \quad (3)$$

Equations 1-3 derived form the foundation of the density-matrix formalism leads to an explicit expression for $\mathrm{CD}_{\mathrm{total}}$. Since relevant derivations are beyond the scope of this review and can be found elsewhere[37, 38, 54, 57], for simplicity, we only give the expressions of the two terms in $\mathrm{CD}_{\mathrm{total}}$. The first term in Eq. 3 is:[37, 38]

$$\mathrm{CD}_{\mathrm{molecule}} = E_0^2 \frac{8}{3} \sqrt{\varepsilon_0} \omega_0 \frac{\Gamma_{12}}{|\hbar\omega - \hbar\omega_0 + i\Gamma_{21} - G_\omega|^2} \mathrm{Im}\left[\hat{P}\boldsymbol{\mu}_{12} \cdot \boldsymbol{m}_{21}\right] \quad (4)$$

where $\hat{P}$ is the field-enhancement matrix at the chiral molecule location, ω_0 and ε_0 are the molecular transition frequency and vacuum permittivity, ω and E_0 are the frequency and electric field of incident light, and Γ_{12} and G_ω correspond to the broadening of native molecular transition and molecule-NC interaction. The second term in Eq.3 is written as:

$$\mathrm{CD}_{\mathrm{NC}} \propto \mathrm{Im}(\varepsilon_{\mathrm{NP}}) \cdot f_{\mathrm{resonant}} \cdot \mathrm{Im}\left(\widehat{K}\boldsymbol{\mu}_{12} \cdot \boldsymbol{m}_{21}\right) \quad (5)$$

where the position-dependent matrix $\widehat{K}$ describes the external field inside the NC, $\varepsilon_{\mathrm{NP}}$ is the permittivity of metal, and f_{resonant} is the coupling strength between the molecular dipole and the NC dipole.

As can be seen from Equations 3-5, the CD spectrum of the hybrid molecule-NC system can be rigorously calculated once (1) the electronic states and orientation of the chiral molecule are given (mostly assumed to be isotropic in the theoretical models) and (2) the field-enhancement matrix $\hat{P}$ and $\widehat{K}$ of the NC, and the molecule-NC coupling strength f_{resonant} are known. Importantly, we are able to identify from these equations several physical implications responsible for chirality transfer: (a) the matrix $\hat{P}$ in Eq. 4 describes the electric field enhancement at the molecular transition frequency at the position of the molecule. Thus, the plasmonic field matrix $\hat{P}$ with nonzero diagonal terms, on the one hand, can greatly enhances the molecular dipole moment ($\boldsymbol{\mu}_{12}$) and, on the other hand, alters the dipole orientation of the molecule, thereby affecting the angle between $\boldsymbol{\mu}_{12}$ and $\boldsymbol{m}_{21}$. This may create an extra CD resonance from a molecule even with mirror symmetry (i.e. $\boldsymbol{\mu}_{12} \perp \boldsymbol{m}_{21}$);[38] (b) the total electric field inside the NC consists of two parts: plasmonic field excited by the incident field and induced field by the chiral molecule dipole, whose interference gives $\mathrm{CD}_{\mathrm{NC}}$. On the one hand, the electric field inside the NC peaks approximately at its plasmon resonance energy. On the other hand, since $\mathrm{CD}_{\mathrm{molecule}}$ is

proportional to $(\omega - \omega_0)^{-2}$ (see Eq. 4) and f_{resonant} in Eq. 5 is proportional to $(\omega - \omega_0)^{-1}$,[37] CD_{NC} therefore decays much slower than $\text{CD}_{\text{molecule}}$ for large detuning ($|\omega - \omega_0| \gg \Gamma_{12}/\hbar$). The above two effects work hand in hand, creating a prominent CD resonance at the NC plasmon band. Considering the fact that high-energy UV light may induce photodamage to many biomolecules, the chirality transfer from the molecular electronic CD in the UV range to the plasmonic CD in the visible range enables non-destructive spectroscopic detection of molecular chirality. (c) Since CD_{NC} is proportional to Δ^{-3} for small molecule-NC separations,[37] which sets a fundamental constraint on the length scale of molecule-NC systems (spanning from a few to tens of nanometres), one can conclude that the above-mentioned electromagnetic interaction is a near-field effect.

2.1.2 Effective polarizability

From a classical point of view, chiral molecules can also be modeled as electric dipoles (here magnetic dipoles are neglected throughout this subsection). An intuitive picture based on this classical assumption is shown in Figure 1(b), where a chiral molecule is treated as a subnanometer particle made of a chiral medium, manifesting its chiral response with different polarizabilities for LCP and RCP lights. The modelling of classical chiral media dates back to 1900s, as Drude reported the first phenomenological studies on optically active media.[58] Followed by Born[59], Fedorov[55] and Tellegen[60], the constitutive equations for a chiral medium have the below forms:[61]

$$\boldsymbol{D} = \varepsilon \boldsymbol{E} - i\kappa_r \sqrt{\varepsilon\mu}\boldsymbol{B} \tag{6}$$

$$\boldsymbol{B} = i\kappa_r \sqrt{\varepsilon\mu}\boldsymbol{E} + \mu \boldsymbol{H} \tag{7}$$

where ε, μ and κ_r are permittivity, permeability and chirality parameter of the medium, respectively. Combining Eqs. 6 and 7 with Maxwell equations, the eigenstates of a plane wave propagating in the chiral medium are $(+)$ LCP and $(-)$ RCP lights with respective effective permittivity written as:[61]

$$\varepsilon_{\pm} = \varepsilon(1 \pm \kappa_r) \tag{8}$$

In addition, since these plasmonic NCs are much smaller than the wavelength of incident light, retardation effects are negligible (i.e., electrostatic approximation applies). The respective effective polarizability α can thus be calculated from Mie theory:[62]

$$\alpha^{\pm} = 4\pi a^3 \frac{\varepsilon_{\pm} - \varepsilon_m}{\varepsilon_{\pm} + 2\varepsilon_m} \tag{9}$$

where a is the radius of the metal NC, and ε_{m} is the dielectric constant of the environment. Since the intrinsic CD of the chiral molecule is relative weak at the plasmonic band (which is equivalent to the density-matrix formalism in which $\text{CD}_{\text{molecule}} \ll \text{CD}_{\text{NC}}$), only dominant CD contribution from the NC's differential absorption is considered. The CD_{NC} can be written as:[39, 63]

$$\text{CD}_{\text{NC}} = A \cdot n_{\text{molecule}} \cdot \text{Re}\left(\int \Delta\alpha \cdot \boldsymbol{E}_0^* \cdot \boldsymbol{E}_{\text{c}} \cdot G(\boldsymbol{r}, \boldsymbol{r}_D)\text{d}V\right) \tag{10}$$

where A is a constant, n_{molecule} is the number of chiral molecules, $\boldsymbol{E}_0$ is the incident field, $\Delta\alpha = \alpha^+ - \alpha^-$ is the difference of LCP and RCP effective polarizabilities, $\boldsymbol{E}_c$ is the local field on the chiral molecule, and $G(\boldsymbol{r}, \boldsymbol{r}_D)$ is dipole-dipole interaction factor, $\boldsymbol{r}$ and $\boldsymbol{r}_D$ refer to the coordinate centers of the NC and the chiral molecule, respectively.

It is noteworthy that effective polarizability is essentially a direct extension of Rosenfeld's equation. In the framework of molecular theories, κ_r can be found to be proportional to the

molecular microscopic parameter β describing the optical activity of the medium:

$$\kappa_r \propto \beta_a = \frac{c}{3\pi h}\Sigma_b = \frac{R_{ba}}{\nu_{ba}^2 - \nu^2} \quad (11)$$

where β_a is the value of β for a molecule in quantum state a, ν is the frequency of incident light, ν_{ba} is the frequency of the light absorbed in the quantum transition jumping from state a to state b, and R_{ba} is rotational strength referring to a constant property of this transition. Eq. 11 is called Rosenfeld equation[56] that connects the classical polarizability description of a molecule with the quantum treatment of its molecular transition.

2.2 Plasmonic fields induced chirality transfer

A close look at Eqs. 5 and 10 reveals that chiroptical activity of a molecule-NC hybrid system can be significantly increased with enhanced electromagnetic fields. Metallic NCs supporting localized surface plasmon resonance (LSPR) provide amplified and tunable plasmonic near-fields.[64-66] In the following subsections, the enhanced plasmonic fields are classified into three categories according to their physical origins: localized fields from isolated NCs,[52, 67-69] near-field hot spots at the gaps of closely-spaced coupled NCs[40, 70-72], and confined fields inside single metal core-shell nanostructures[73, 74]. By placing chiral molecules at these locations of enhanced plasmonic fields, the molecular chirality can be grafted to the plasmon resonance bands of the metal nanostructures, exhibiting CD signal intensities several orders of magnitude larger than that of the intrinsic molecular CD at the same wavelength bands (and comparable to that of the intrinsic molecular CD in the UV region).[40, 52, 67-69, 74-79]

2.2.1 Localized fields induced CD in isolated NCs capped by chiral biomolecules

Single metal NCs are fundamental building blocks for plasmonic complexes. Theoretical calculations by Mie theory indicate that the electromagnetic field of a smooth particle (e.g., spherical and ellipsoid) reaches the maximum at the particle surface.[62] Therefore, it is convenient to achieve enhanced CD signals by attaching chiral biomolecules such as cysteine (Cys),[80] peptide,[52, 68] protein,[81, 82] and DNA[83, 84] to the surface of plasmonic NCs. For instance, Lieberman *et al*. reported two orders of magnitude enhancement in CD response in the visible by coating Ag nanospheres with L-GSH and bimane chromophores complexes (**Figure 2**a);[85] Katz and coworkers demonstrated a similar observation by bonding chiral calix[4]arene ligands on the surface of gold (Au) nanospheres.[86] These observations were soon confirmed by Govorov and coworkers both theoretically[38] and experimentally in a similar system.[52] Based on this system, they also found that the enhanced chiroptical response could be tuned by varying the NC/molecule molar ratio.[67]

Plasmonic fields of non-spherical metallic NCs are more complicated, because they may support multipolar plasmon modes with complex near-field distribution profiles.[87] Nevertheless, the electric dipole resonance is still the leading mode given that the NCs are sufficient small (which means the retardation effect can be neglected).[62] In this case, the induced CD signal intensity follows $\mathrm{CD_{NC}} \sim 1/R^3$,[37] where R is molecule-NC center-to-center distance. For example, Zhu *et al.* showed enhanced CD signals from both the dipolar transverse and longitudinal LSPR modes of Au nanorods (NRs) coated with cysteine molecules (**Figure 2**b).[70] When it comes to plasmonic NCs with sharp edges or apexes,

the local plasmonic fields can be significantly leveraged with preferred orientation. Levi-Belenkova *et al.* found that the chiral-molecule-induced plasmonic CD strongly depends on the orientation of chiral molecules adsorbed on the surface of silver (Ag) nanocubes, which cannot be explained by the simple plasmon-molecule dipolar interaction model but has to resort to the multipolar nature of the plasmon modes involved.[88] In fact, Lu and co-workers had observed a similar phenomenon in gold/silver core/shell nanocubes adsorbed by single-stranded DNA molecules, showing two orders of magnitude enhancement of CD signals in the violet region (**Figure 3**a).[89] In this study, they changed the alignment of DNA on the cube surface by varying the solution ionic strength. When the DNA molecular orientation is perpendicular to the cube surface, a strong plasmonic CD signal appears. In sharp contrast, when the DNA molecules are randomly oriented on the cube surface, there is no detectable CD signal. Another interesting study illustrated in **Figure 3**b demonstrated an enhanced chiroptical activity in the visible and near-infrared regions by capping achiral gold nanorods with chiral-molecules-filled mesoporous silica.[69]

2.2.2 Near-field hotspots amplified CD in molecule-connected coupled NCs

In the persistent quest for further enhancing plasmonic near-fields, one design concept has proven to be exceptionally efficient, that is, generating plasmonic near-field hotspots. Plasmonic hotspots can be found in the tiny gaps of closely-spaced metal NCs, yielding extremely small mode volumes (down to $10^{-7}(\lambda/n)^3$)[90] and highly intensified fields. Such field localization and enhancement can significantly boost light-matter interactions and has been widely exploited in surface-enhanced Raman spectroscopy (SERS),[91-93] plasmon-enhanced spontaneous emission,[94] and plasmonic biosensing[93, 95, 96] etc. As for chiroptical effects, placing chiral molecules inside the nanoscale gaps of coupled metallic NCs, such as linearly connecting achiral metal nanospheres into oligomer chains, can produce up to two orders of magnitude CD signal intensity enhancement.[71, 97]

Besides spherical nanoparticles (NPs), plasmonic hotspots built from metallic NRs have also been under intensive study as their structural geometries, field enhancement factors and resonance frequencies can be tuned at will.[98] Nanometer-sized gaps can be formed in NR assemblies with two typical configurations, namely end-to-end (ETE) and side-by-side (SBS) as illustrated in **Figure 4**a. Both configurations sustain two hybridization plasmon modes, a low-energy symmetric bonding mode and a high-energy asymmetric antibonding mode (**Figure 4**b).[64, 65, 99] Since the antibonding mode is extremely dark and cannot be efficiently excited, plasmonic enhancement in these NR assemblies mainly comes from the bonding mode. Intuitively, if all the nanorods of same dimensions lay at the same plane (e.g., on the surface of a flat substrate), ETE and SBS structures would not have intrinsic chirality. However, Tang's group reported that the ETE assemblies of gold NRs with chiral Cys or GSH exhibit strong CD signals, which can be manipulated from 500 nm to 900 nm by changing the aspect ratio of the Au NRs.[70] Similar studies were also reported by other research groups.[72, 75] Varying the concentration of surfactants in the Au NR solution can also produce SBS structures,[73] which were found to exhibit even larger CD signals than the ETE counterparts.[40] This difference is attributed to the larger surface area of the SBS configuration, which allows a larger amount of chiral molecules to reside in the gap areas. Recently, Lei's group reported an observation in contrary to Tang's result, where the ETE-

assembled Au@Ag core-shell NRs show larger plasmonic CD signals than the SBS-assembled ones (**Figure 4**c).[39] They found that the chiroptical enhancement is essentially a competition between the number of chiral molecules and local field enhancement in the gaps, as revealed by Eq. 10. The gap distance of their Au@Ag assemblies is much smaller than Tang's structures, and Ag-based nanostructures usually possess stronger plasmonic fields than Au-based ones of the same structural parameters. These two effects work hand in hand, creating stronger plasmonic hotspots in the ETE assemblies, overcoming the reduced number of chiral molecules located in the hotspots and consequently yielding a larger anisotropic factor in the ETE configuration.

DNA origamis have been reported to be an alternative class of connecting molecules for construct plasmonic nanogaps with more flexibilities.[100-102] Kneer *et al.* systematically studied the impact of gap size, material composition and particle geometry on the chirality transfer effects in DNA-assembled metal nanostructures,[102] revealing that the CD signal transferred to the plasmonic frequency domain is most intensive for systems with strong near-field hotspots. Interestingly, such plasmonic CD response can be reversed back and forth by temperature-dependent assembly and disassembly of DNA-assembled Au NRs:[100] at low temperature (20 °C), the double-stranded (ds) DNA molecules are complementary to each other, leading to the formation of SBS-assembled Au NRs with strong CD signals in the visible region; when the temperature increases to above 60 °C, dsDNA molecules melt in the solution and the Au NRs disassemble, causing the disappearance of plasmonic CD due to the reduced local field enhancement.

Among those chiral biomolecules-assembled coupled NCs, plasmonic heterodimers made of different types of metal NCs (composition and shape) have attracted particular attention because their nanogaps could generate stronger plasmonic fields than that of plasmonic homodimers.[103] Xu's group demonstrated Au NR-NP heterodimers linked by chiral dsDNA (**Figure 4**d),[104] whose plasmonic CD band could be tuned from 520 nm to 750 nm by simply adjusting the length of dsDNA. Similarly, Kotov *et al.* showed that deposition of Au or Ag shells around NP heterodimers enables chiroptical spectral tunability and enhanced optical activity (**Figure 4**e).[105] Based on the observed shift of CD band, it was concluded that engineering of shell thickness and composition provides the possibility for controlling both amplitude and frequency of the plasmonic CD band in the NP heterodimers.

2.2.3 Shell engineering of plasmonic CD in molecule-filled core-shell nanostructures

Metallic core-shell nanostructures, which have recently gained increasing interest from the chiral plasmonics community,[106, 107] are another type of plasmonic systems that provide high degrees of resonance tunability and tightly confined near fields. In a bimetallic core-shell NP, the plasmon hybridization between the inner sphere and the outer shell enables flexible tuning of its optical responses, including resonance frequency, line shape, field localization, absorption and scattering efficiencies, making such plasmonic NP even more versatile for manipulating plasmonic CD than the above-discussed nanostructures.[108-111] Hao *et al.* reported that structurally achiral gold-gap-silver NPs can exhibit pronounced plasmonic CD bands when their interior nanogaps are filled with chiral cysteine (**Figure**

5a),[112] and that the CD signal strongly depends on the gap size that can be controlled by adjusting the amount of cysteine. Hou *et al*. also reported that cysteine-modified Au NRs with Ag shells (i.e. Au@Ag core-shell NRs) show strong plasmonic CD signals, whereas their spherical counterparts have no detectable optical activity (**Figure 5**b).[76] Similarly, Xu's group synthesized discrete chiral Au@AgAu yolk-shell NRs starting with penicillamine molecule-modified Au NRs (**Figure 5**c),[113] and found that their plasmonic CD response can be regulated by changing the aspect ratio of the Au NRs, revealing that structural anisotropy plays a key role in the plasmonic CD enhancement of these core-shell nanostructures.

Shell engineering represents another approach for controlling plasmonic CD enhancement in chiral molecule-filled core-shell metal NPs. Recent experiments have showed that chiral molecules have a significant impact on the formation of metallic shells. Wu *et al.* found that gold core-DNA-silver shell NPs exhibit an intense and robust chiroptical response in the visible region, where hybrid DNA-Ag shells were prepared by Ag overgrowth on the DNA template (**Figure 5**d).[114] Similar approach was also adopted by Yan *et al*. to synthesize starfruit-like chiral Au NPs via cysteine-mediated overgrowth of Au on Au NRs (**Figure 5**e).[115] Recently, Zheng *et al*. embedded chiral molecules in Au core-shell NRs and observed that the NR morphology is governed by the amount of cysteine used (**Figure 5**f):[116] high concentration of cysteine molecules produces multiple irregularly arranged spikes on the shell. Notably, the introduction of such irregular morphologies on the shells, either chiral or achiral, leads to superior chiroptical responses from the core-shell NRs.

2.3 Other types of electromagnetic interactions responsible for chirality transfer

Although electromagnetic dipole-dipole interactions in the near field regime appear to be the most efficient means for chirality transfer, one drawback still remains in this model: the interaction distance between a chiral molecule and a metal nanostructure spans only a few nanometers. In other words, the "active region" of the metal nanostructure is such small that only a few chiral molecules could reside in and contribute to the induced plasmonic CD signals, which cannot explain several recent experimental observations[54, 117, 118]. Therefore, two new physical mechanisms, namely long-range electromagnetic interaction and through-space chirality transfer, stand out and offer insightful guidelines in the design and application of chirality-transferred plasmonic nanostructures.

2.3.1 Long-range electromagnetic interaction

Chirality transfer through long-range electromagnetic interactions was observed for the first time by Abdulrahman and co-workers:[117] the coupling distance between chiral molecules and metallic nanostructures can be as large as several hundred nanometers. In general, the long-range electromagnetic interaction refers to the phenomenon that chiral molecules interact with achiral plasmonic nanostructures through far-field electromagnetic coupling scaled by $1/R$.[119, 120] Although the radiative couplings between resonant plasmonic or dielectric nanostructures have been studied for years,[119, 120] it is contourintuitive to observe this effect between subnanometer molecules and plasmonic structures. As shown in **Figure 6**a, depositing a thin layer of chiral biomolecules on an

array of achiral Au nanocrosses produced a new CD band near the plasmon resonance frequencies. Theoretical calculations showed that the induced CD signal intensity is proportional to the thickness of the chiral layer,[117] implying that the chiral molecules located at distances of the order of λ from the plasmonic nanostructures can still contribute to CD enhancement (**Figure 6**b). Detailed derivations of long-range electromagnetic interactions are documented in Ref. 54.

2.3.2 Through-space chirality transfer

In addition to the above-discussed chirality transfer from chiral biomolecules to achiral metal nanostructures, the chiral information of biomolecules may also be transferred to achiral molecules through plasmon-mediated through-space chirality transfer. For example, Ostovar pour *et al.* reported that the stereochemical response of a chiral analyte can be transmitted to an achiral benzotriazole dye through an achiral SiO_2 shell (3-5 nm thick) coated on an achiral silver NP (**Figure 6**c).[118] Although the chiral analyte molecules adsorbed on the SiO_2 shell are not in direct contact with the Ag NP surface, the NP acts as a "plasmonic transmitter" in which the local chiral currents induced by the chiral analyte can be conveyed to the achiral dye reporters, generating surface-enhanced resonant Raman optical activity. Although this phenomenon features a long-range interaction, similar to the $1/d$ dependence reported by Abdulrahman *et al.*,[117] it cannot be explained by the radiative coupling mechansim and does not require the presence of superchiral fields, and deserves further in-depth studies to understand the exact physical mechanism responsible.[121]

3. Biomolecule-guided chiral assembly and growth of metal nanostructures

Inspired by the fundamental concepts and tremendous exciting findings in stereochemistry, plasmonic nanostructures acting as nanoscale building blocks can be assembled to replicate those phenomena originally observed in molecule systems.[122] In addition, theoretical studies have shown that structural chirality from plasmonic nanostructures can generate exceptionally strong chiroptical effects in the visible and near infrared regions,[123-127] with chiroptical signals several orders of magnitude larger than that induced by chiral molecules through electromagnetic interactions. Therefore, many bottom-up approaches, in analogy to those used for molecular assembly of inorganic materials,[128-131] have recently been developed to realize large-scale plasmonic entities with structural chirality. In this section, several self-assembly approaches, including chiral templates and DNA origami, will be discussed in the context of chiral assembly of plasmonic nanostructures.

3.1 Chiral assembly of metal nanostructures with definitive chiral geometries

3.1.1 Chirality transfer via chiral templates

Chiral templates are patterned structures that can be used to organize metal NPs into chiral assemblies.[132] Typical chiral templates include chiral fibers,[133, 134] peptides,[135-141] organogelators,[142-144] liquid crystals,[145-149] and chiral mesoporous silica (CMS) etc.[150-153] With the use of twisted supramolecular fibers, Liz-Marzán's group succeeded in assembling gold NRs in an helical arrangement (**Figure 7**a),[133] observing a giant CD

signal of up to ~190 mdeg. Specifically, the Au NRs were adsorbed onto the scaffold of the twisted fibers through non-covalent interactions. The formed NR-fiber superstructure has a length of up to a few micrometers, which facilitates an efficient interaction between the incident light and the Au NRs and consequently results in the unprecedentedly high levels of anisotropy factor. Peptides are another suitable helical architectures that can be engineered to fabricate chiral superstructures. For instance, Wang and co-workers demonstrated the first peptide-template-based helical arrays of metal NPs,[154] where negatively-charged Au NPs are attached on the peptides through electrostatic attraction. Interestingly, adjusting the pH value could change the resulting structure from single-chain to double-helical arrays with structural tunability.[155] Later on, Rosi's group constructed a highly aligned double-helical superstructure of Au NPs by using alkyl-chain terminated oligopeptides.[135] With delicate control over inter-particle spacing and particle size, the helical pitch and the resultant overall handedness could be precisely tuned (**Figure 7**b).[136]

In addition to twisted fibers and peptides, organogelators, a kind of hydrogel templates, have also been widely used for producing chiral plasmonic superstructures.[142-144] Since controlled growth of metal NPs along the organogelators can be achieved by UV reduction of noble metal ions on the supramolecular templates (**Figure 7**c),[144] the resulting NP superstructures with significant inter-particle couplings and well-defined helicity exhibit remarkable structural chirality with tunable CD signals, rendering a fast and high-yield fabrication method for chiral nanomaterials.

On the other hand, liquid crystals have also been widely exploited for fabricating helically arranged plasmonic superstructures.[145-148, 156-158] Because cellulose nanocrystals (CNCs) are negatively charged, high-aspect-ratio rod-like metallic NPs can assemble in cholesteric liquid crystalline phases. Based on this principle, Querejeta-Fernandez *et al.* demonstrated the fabrication of chiral nematic films of CNCs loaded with Au NPs (**Figure 7**d),[148] where the CNCs offer host sites for assembling the guest Au NPs with tailorable orientation control. As a result, surprisingly high plasmonic CD of up to $\sim 10^3$ mdeg was achieved in the Au NP loaded chiral CNC films.

Finally, twisted CMS processing a hexagonal surface and helical pore orientation has also been found particularly efficient in chiral assembly of plasmonic NPs. In this aspect, Che and coworkers reported the use of highly ordered CMS for creating strong plasmonic CD enhancement (**Figure 7**e).[153] through the in situ growth of achiral Ag NPs in CMS, they realized 3D helical arrangement of the NPs and observed a large CD enhancement due to asymmetric plasmon-plasmon interactions between Ag NPs in the chiral environments, with the helical pore orientation predominantly responsible for the induced CD.

3.1.2 Chirality transfer via DNA-guided self-assembly

Different from those aforementioned chiral templates, DNA molecules process unique programmable Watson–Crick base pairing and have become one class of the most promising candidates for controllable assembly of metallic NPS.[159, 160] By rationally designing the length and sequence of DNA molecules, metallic NPs can be easily assembled into various chiral configurations, including helical, triangular, pyramidal and

octahedral structures.[161-165] In such chiral assembly, spherical NPs are often preferred because of the relaxed requirement on orientation manipulation. To the best of our knowledge, Alivisatos and co-workers reported for the first time the fabrication of Au NP assemblies by using dsDNA as molecular linkers.[164] In their study, four Au NPs of different sizes were rigidly connected respectively to the tips of four dsDNA molecules, yielding a pyramidal configuration without a center of symmetry. Later, Kotov *et al.* demonstrated a pyramidal grouping of two Au NPs, one Ag NP and a quantum dot (QD) with the assistance of DNA strands (**Figure 8**a).[165] The chiral pyramid displays strong chiroptical signals ranging from 350 nm to 550 nm, and can be potentially extended to the NIR region by using narrow-bandgap QDs. Recently, Xu's group reported a propeller-like nanoscale tetramer with an upconversion nanoparticle (UCNP) located at the center of three Au NRs (**Figure 8**b).[166] This hybrid chiral tetramer was fabricated by DNA-driven complementary self-assembly of three DNA-decorated Au NRs and a DNA-decorated UCNP. On the one hand, the CD response of these hybrid tetramers can be readily tuned in the visible region by varying the lengths of DNA linkers, aspect ratios of Au NRs and sizes of UCNPs. On the other hand, the upconversion luminescence signal of the system can be dramatically enhanced by more than 20 times in aqueous environment by sophisticatedly manipulating the distance between the UCNPs and Au NRs.

Long DNA scaffold strands can be folded into 2D or 3D shaped DNA origami,[167, 168] which is regarded as a breakthrough of DNA nanotechnology. Many studies have shown that DNA origami can rigidly direct metallic NPs into self-assembled plasmonic superstructures.[167, 169-174] Based on this principle, Liedl and coworkers who utilized DNA origami 24-helixs bundle to create helix-like plasmonic superstructures with defined number of 10 nm Au NPs (**Figure 8**c),[169] which probably represents the first demonstration of constructing helical arrangement of metallic NPs by using DNA tiles. Since then, DNA origami has emerged as a versatile and viable platform for generating self-assembled chiral plasmonic superstructures.[175] For instance, Shen *et al.* organized four spherical Au NPs into a 3D tetramer configuration by employing a rectangular DNA origami (**Figure 8**d),[170] where the position of the bottom NP relative to the top three ones determines left- or right-handedness of the configuration. By taking advantage of the anisotropic geometry of Au NRs and precisely tuning the attachment sites of bifacial DNA origami, Lan *et al.* were able to create 3D anisotropic Au NR dimers,[176] which exhibit a spatial-configuration-dependent plasmonic chiral response tailorable in the visible region.

Another unparalleled advantage of DNA origami for chiral assembly of metallic NPs is the reconfigurable capability under external physical or chemical stimuli.[177-179], which makes dynamic modulation of chiroptical activity possible by imparting reconfigurability and functionality to originally passive plasmonic systems. As shown in **Figure 8**e, a 3D plasmonic cross-like nanostructure consisting of two Au NRs can be created by hosting the NRs on a switchable DNA origami template made of two connected bundles.[180] By tuning the angle subtended by the two bundles through two DNA locks and hence the relative angle between the Au NRs, the conformation of the system can readily be switched between left-handed, relaxed, and right-handed, enabling the plasmonic nano-cross as an optical reporter for transducing its conformational changes into CD changes at visible wavelengths. Similarly, Lan *et al.* also fabricated a 3D plasmonic superstructure consisting of Au NRs

attached on a DNA origami supramolecular polymer.[181] As depicted in **Figure 8**f, Au NRs functionalized V-shaped DNA origami are assembled into a hierarchical stair helix with a pinwheel end view with each origami arm connected by a Au NR through complementary DNA hybridization. Because the hinge region of the origami can be reconfigured dynamically through toehold-mediated strand displacement, the angle of the V-shaped DNA origami can be altered and hence the Au NR superstructure can be switched between a tightly folded and an extended state, i.e. between left-handed and right-handed chiral states. More interestingly, the DNA origami based NP assembly has recently been extended to produce plasmonic stereoisomers with up to three chiral centers, yielding eight origami-Au NR stereoisomers[182] and thus providing a viable means for nanostructure assembly with high fidelity and dynamic controllability.

3.2 Chirality transfer induced growth of intrinsically chiral metallic nanostructures

Although the chiral template-assisted self-assembly of achiral metallic NPs into plasmonic superstructures can generate pronounced, tunable chiroptical activities as discussed in Section 3.1, intuitively, individual metal nanostructures with chiral geometries should as well display intrinsic chiroptical effects.[127] As shown in **Figure 9**a, theoretical calculations show that two surface deformed Au NPs, 'twister' and 'anti-twister', exhibit enhanced CD signals at their plasmon resonance bands.[127] Therefore, the direct wet-chemical growth of isolated chiral metallic nanostructures may represent a more straightforward approach to obtain large-scale plasmonic nanostructures with giant optical chirality. In fact, inorganic NPs decorated with chiral surfactants have long been used as "seeds" for chemical growth of chiral superparticles.[183] In this section, we discuss two growth methods to synthesize intrinsically chiral NPs in chiral environments: (1) precipitates reaction of metallic particle 'seeds' under the guidance of chiral molecules; (2) using intrinsically chiral semiconductor NCs as chiral seeds to grow chiral metal shells and hence produce mteal@semiconductor chiral hybrids.

Earlier studies on chemical growth of plasmonic nanostructures in an aqueous solution of chiral supermolecular structures revealed two plasmonic CD induction mechanism: (a) small Ag NPs adsorbed by large stacks of chiral biomolecules exhibit induced CD at the NP plasmon absorption band, and the CD signal decays together with the UV CD band of the molecules on heating the solution; (2) however, larger Ag NPs adsorbed by a monolayer of chiral molecules show temperature-insensitive plasmonic CD that is too strong to be induced by the low chiroptical response of the molecular monolayer, implying that the large plasmonic Cd response may result from a subtle chiral shape distortion of the Ag NPs.[67] Recently, the second mechanism was unambiguously verified by Lee *et al.* who reported the growth of outspread petal-like chiral Au nanostructures with two-dimensional twisted morphologies as illustrated in **Figure 9**b.[184] In the growth process, the chiral GSH molecules were consecutively attached on the surface of Au seed NPs to modulate the growth direction of the each nano-petal and hence influence the macroscopic shape of the resultant largely curved Au nanostructures.[185] Later on, the same group extended their synthesis strategy to prepare plasmonic helicoids (**Figure 9**c),[186] where Cys molecules were used as additives in the two-step seed-mediated growth procedure, leading to the formation of "kink" sites in the resultant NPs showing extremely large CD signals of up to

500 mdeg when dispersed randomly in solutions. Lee's synthesis method is remarkably simple for the preparation of shape-designed metallic NPs, providing a viable means to artificially design and fabricate 3D chiral plasmonic nanostructures.

In addition to molecular chirality-guided growth of chiral metallic nanostructures, chiral surfactant molecules can also be used for enantioselective synthesis of intrinsically chiral semiconductor NCs, which can be further utilized as chiral seeds for the growth of chiral metallic shells. For instance, Ben-Moshe *et al.* reported the synthesis of chirality-selective mercury sulfide (α-HgS) NCs by using penicillamine as chiral surfactant molecules,[187] and the induced high enantioselectivity probably originates from binding of the surfactant thiolate groups to Hg ions in the formed crystal. Following a similar approach, the same group also synthesized colloidal tellurium (Te) and selenium (Se) NCs which both have the same space group as α-HgS.[130] They then used the Te and Se NCs as chiral seeds to grow Au or Ag nanostructures (**Figure 9**d), and surprisingly observed that the seeds can transfer their chirality to the newly formed Au and Ag nanostructures with obvious chiroptical responses at their respective plasmon absorption bands, offering a new yet simple approach for chirality transfer.

4. Molecular conformation change induced chirality transfer

When a chiral molecule is adsorbed onto the surface of a metal NP via hydrogen bonding, conformational changes may take place in the molecule. For instance, the interaction between a citrate-capped Au NP and islet amyloid polypeptide (IAPP) triggered the IAPP conformational transition from random coil to ordered structures.[188] Scientists have observed similar phenomena in molecule-plasmon chirality transfer processes, that is, metallic nanostructures induce the adsorbed chiral molecules to deform their conformation and rearrange, and consequently inducing CD response in a wavelength band different from the original CD band of dispersed molecules. For example, Liu *et al.* observed newly emerged CD signals from chiral biomolecules conjugated with Ag NPs in the UV band (**Figure 10**a).[189] This effect, originated from the synergetic interplay between CO_2^- and NH_3^+ groups, leads to a chiral molecule-protected Ag NPs both in UV and plasmonic band. Li *et al.* reported a similar results, and in addition, observed that molecule-Au NP complexes does not feature this phenomenon.[190]

A recent study reported by Bao *et al.* also observed a similar phenomenon where an atypical strong CD response is generated in the Au@Ag core-shell nanocuboids Cys system (**Figure 10**b).[63] By comprehensive investigations on the effects of solution temperature, pH value and external ions, the linkage of CO_2H group and NH_2 group of vicinity Cys molecules via hydrogen bonding is attributed to the cause of new CD band. Synergetic interplay of the electrostatic interaction among the R side chains and the $Ag^+ \cdots Ag^+$ argentophilic attraction are two interactions that may be responsible for the new induced CD signals.[191, 192]

The molecule conformation of biomolecules that directed by noble metals, can further be

regulated via external chemical stimuli, and as a result, creating additional chiroptical responses. For instance, in addition to the CD signal caused by Ag-GSH interaction and located 200-250nm, Markovich *et al.* observed a new chiroptical response at 280nm when reducing the solution's pH from 5 to 4.5 in GSH-Ag nanocube system (**Figure 10**c).[193] This effect, probably attributed to the creation of disulfide bonds based on surface-catalyzed oxidative coupling,[194] leads to the formation of diglutathione.

5. Optical chirality based advanced biosensing and bioimaging

One of the most intriguing features of chirality transfer probably lies in its ability to "boost" the chiroptical signals of biomolecules, which opens an avenue for chiral detection based biosensing and bioimaging. In this section, several chiroptical response-based sensing and imaging strategies together with relevant chirality transfer mechanisms are summarized.

5.1 Biosensing application

Generally speaking, chirality-based sensing outperforms most of conventional refractive index-based sensing techniques as it can collect additional higher-order hierarchical information from biological macromolecules, such as secondary (α-helices and β-sheets) and tertiary structures (formed via interactions between amino acids) while simultaneously preserving refractive index-sensing capabilities. So far, the above-discussed three chirality transfer mechanisms have been used to develop new sensing platforms for detecting chiral biomolecules, such as peptide, DNA, RNA, etc.[195-197] A summary of sensing mechanisms and corresponding limits of detection (LOD) is given in **Table 1**.

For chirality-based recognition and quantification of enantiomers, a linear dependence of CD signal on the concentration of target analyte is an essential prerequisite for convenient operation. In this context, Xu *et al.* utilized the plasmonic near-field hotspots in Au NP dimers to recognize and quantify the concentration of cysteine enantiomers,[198] and observed a linear dependence of CD signal with a detection limit of 20 pM for L-cysteine. On the other hand, molecular conformational transformation enables chiral discrimination in the UV band, which does not rely on the induced plasmonic CD as used in the former case. With the help of mesoporous silica coated Ag NPs (Ag@mSiO_2), Wang *et al*. reported the discrimination of enantiomeric cysteines (L- and D-) by monitoring the new mirror-like CD bands appeared in the range of 240 – 350 nm.[199] Importantly, the formation of cysteine-Ag@mSiO_2 supramolecular networks by electrostatic attraction and hydrogen bonding enables a LOD as low as 12.5 μM, which surpasses conventional electronic CD measurement techniques considerably.

Guided self-assembly of plasmonic NCs is probably one of the most popular sensing strategies for chiral recognition of DNA and microRNA (miRNA), because molecule-directed structural chirality provides significantly enhanced CD signals. For instance, Kotov *et al.* demonstrated that twisted SBS and ETE assembled Au NRs could enable ultrasensitive DNA detection with a remarkable LOD (as low as 3.7 aM, **Figure 11**a).[200] Later on, the same group extended the concept to a heterodimer system (**Figure 11**b),[201] and surprisingly achieved a record LOD of 15 zM for cancer biomarkers (prostate-specific

antigen), which is approximately 2 times lower than the most sensitive method at that time.

In addition, chiral plasmonic assemblies also exhibit exceptionally high sensitivities in chiroptical response to structural distortion and environmental alteration[202] and hence an induced subtle conformational change could even invert the handedness of a specific helicoid nanostructure.[123, 126] **Figure 11**c presents an interesting example in which DNA-bridged NP dimers flip their handedness when moving from interstitial fluid to cytosol in a model cell.[203] In this study, Sun *et al*. demonstrated the localization (intra-/extracellular) of NP dimers could be determined via the induced CD signals, and they concluded that this effect was largely due to the change of equilibrium conformation of the assemblies defined by inter-dependent electrostatic, elastic, and van der Waals interactions. Later, the same group also realized spatially resolved chiral detection of intracellular miRNA sequences in living cells by self-assembled SBS Au NR dimers (**Figure 11**d).[204] This was achieved by coating the surface of Au NRs with poly(styrene-b-acrylic acid) and modifying them with cell-penetrating peptides to provide intracellular stability and biocompatibility, and then transporting the modified Au NRs through the cellular membrane to induce detectable CD signals via the immediate intracellular self-assembly of Au NRs into the SBS dimers. The dynamic assembly of chiral NRs dimers in living cells was also confirmed by SERS and fluorescence resonance energy transfer.

Finally, as chiral assembly of plasmonic nanoarchitectures has been developed as a mature and powerful sensing platform for chiral biomolecules, it is convenient to extend this concept to other biomolecule-based recognition techniques. For example, in the presence of heavy metal ions such as Hg^{2+} and Ag^{+}, DNA skeletons can form stable T-Hg^{2+}-T and C-Ag^{+}-C covalent bonds. Recently, Yan *et al*. demonstrated a reusable Hg^{2+} sensing platform based on plasmonic heteropyramids made by self-assembling Au NPs and ssDNA sequences,[205] and observed a LOD as low as 0.2 pg mL^{-1} in the low-concentration linear response range.

5.2 Bioimaging applications

In addition to biosensing applications, the small size yet extraordinary strong optical activity of chiral self-assembly nanostructures promises a vast research space in interdisciplinary areas such as pharmacology, biology, as well as physiology. Bioimaging aims to visualize biological process *in vivo* with non-invasive measurements. In principle, chirality-based bioimaging takes advantage of the activatable feature of metallic NCs that can be immobilized with biological macromolecules. For instance, Gao *et al.* reported a new class of photodynamic therapy agent, namely, self-assembled shell–satellite nanostructure, that features intense optical activity with high phototherapeutic effect for cancer cells under RCP light (**Figure 12**a).[206] The shell-satellite hybrid, composed of silver NP core and gold NP satellite linked by DNA sequences, not only has high reactive oxygen species generating efficiency, but also features a promising imaging agent for X-ray computed tomography and photoacoustics imaging.

On the other hand, bioimaging also exploits the self-assembly, or dissociation, of the chiral plasmonic NCs configurations, yielding high signal-to-noise on/off ratio of chiroptical

response that permits real time imaging and high spatial resolutions. For example, Xu's group reported the fabrication of self-assembled nanopyramids that are capable of real time visualization of intracellular miRNA **(Figure 12**b).[207] The nanopyramids, consisting of two Au NPs and two UCNPs, exhibit giant plasmonic chirality and weak upconversion luminescence (UCL). In sharp contrast, with the presence of target miRNA molecules, nanopyramids dissociate into isolated components, yielding strong UCL with no detectable CD signals. As shown in **Figure 12**c, this important feature, responsible for the confocal imaging and *in situ* quantification of miRNA in live cells, permits much higher sensitivity than conventional luminescence detection method. Later on, the same group extended this strategy to *in vivo* imaging of the polymyxin-B-resistant *Escherichia coli* based on a plasmonic chiral heterodimers system.[208] The heterodimer possesses a polymyxin B modified UCNPs and an anti-polymyxin-B-antibody coupled gold yolk–shell nanoparticle (YS NPs), featuring the same optical properties as the above-discussed nanopyramids both in their assembled and dissociated configurations (**Figure 12**d). Owing to the high (low) affinity between UCNPs and polymyxin-B-sensitive (resistant) strain membrane that response for the high (low) intracellular and low (high) extracellular UCNPs concentrations, the authors managed to obtain the level of polymyxin-B-resistant bacteria by analyzing both CD and UCL signals. As a result, the polymyxin-B-resistant level in infected living mice can be quantified and visualized in only 8 hours by time-dependent *in vivo* UCL imaging techniques (**Figure 12**e), which is about one-third in time compared with conventional minimum inhibitory concentration method.

6. Conclusion and Future Outlook

Chirality possesses fascinating characteristics in nature not only for its geometric property, but also the symmetry considerations in fundamental physics. In this review, we have summarized the chirality transfer mechanisms from subnanometer biochemical molecules to submicrometer plasmonic metastructures in three aspects. In fact, all these mechanisms may work hand in hand and contribute to final chiroptical effects, which is of particularly difficult for researchers to interpret. For example, aluminum nanoparticle dimer provides strong electromagnetic enhancement in UV band.[209] Therefore, chiral molecule may experience both conformational changes and dipole-dipole interactions once attached to aluminum surface. It is noteworthy that special care should be taken as the CD signal at plasmonic band, originated from dipole-dipole interactions, is probably intertwined with structural chirality.[210, 211] For instance, when two NRs are assembled together as a plasmonic dimer, they may not reside in the same plane, forming structural chirality.[212, 213] The chiroptical enhancement of nanostructure therefor is a competition between electromagnetic interaction and structural chirality,[214] which cannot be differentiated by traditional ensemble measurements. Link and coworkers recently conducted an in-depth measurement on plasmonic monomer and dimer NR-bovine serum albumin (BSA) complexes using single-particle circular differential scattering spectroscopy with correlated tomographic reconstruction.[210] They confirmed that chiral NP dimer, benefitting from both structural chirality and dipole-dipole interaction, exhibit a strong CD signal. Interestingly, while achiral dimer demonstrates a medium CD enhancement, single NC-BSA complex has no detectable CD signals. This experiment solves a long-term question that how do structural chirality and dipole-dipole interactions contribute to final

CD spectra.

Chirality is mostly associated a geometric property, whereas chiroptical effect lies within the regime of light-matter interaction, namely, an object transfers its geometrical information to electromagnetic fields. However, point-to-point correspondence between geometric chirality and the asymmetry of electromagnetic field (i.e., optical chirality) is still elusive. Intuitively, helicoid configurations such as sub-wavelength nanohelices could be a promising candidate, though even minute geometric distortion results in the flipping of optical chirality.[123, 126] Until now, the symmetric requirement of an isolated nanoparticle with high-performing chiroptical response have kept an open question for both theoretical investigations and fabrication considerations.

The fast growth of this field imposes an urgent need on rational and advanced synthesis of chiral structures. Recently, CD near unity material is fabricated through top-down techniques with high accuracy.[215, 216] However, low-cost and large-scale synthesis of chiral material are the basic prerequisites that prohibit these techniques for practical applications. Alternatively, bottom-up approach enables scalable and economical syntheses, but at the cost of flexibility and accuracy. Within this context, high yield, accurate fabrication yet strong chiroptical plasmonic nanostructures is still an overarching challenge for bottom-up approach. Crucially, there have been some remarkable advances in this field including chiral molecule-directed synthesis and reconfigurable DNA origami templates.

To conclude, the field of chiral plasmonics has just entered a fast-development phase not only from the theory, synthesis and application point of view, but also interdisciplinary areas.[217] We anticipate that these directions will be the key for creating solutions to long-standing challenges for future development.

Acknowledgements

Dr. Z. L. Cao and Miss H. Gao contributed equally to this work. We acknowledge the City University of Hong Kong (Project No. 9610434), the financial support from the Hong Kong Polytechnic University (Project No. 1-ZVH9), the Research Grants Council of Hong Kong (GRF Grant No. PolyU 152603/16E), the Hundred Talents Plan of Sun Yat-sen University (Project No. 76120-18841200), and the National Natural Science Foundation of China (Grant No. 61905290).

Received: ((will be filled in by the editorial staff))
Revised: ((will be filled in by the editorial staff))
Published online: ((will be filled in by the editorial staff))

Reference

[1] W. T. B. Kelvin, *Baltimore Lectures on Molecular Dynamics and the Wave Theory of Light*, Cambridge University Press, London, UK 1904.
[2] L. Pasteur, Ann. Chim. Phys. **1848**, 24, 442.
[3] J. Gal, Nat. Chem. **2017**, 9, 604.
[4] M. Uwe, *Amino Acids and the Asymmetry of Life: Caught in the Act of Formation*, Springer, Berlin 2008.
[5] K. M. Rentsch, J. Biochem. Bioph. Methods **2002**, 54, 1.
[6] W. Walther, T. Netscher, Chirality **1996**, 8, 397.
[7] J. D. McGarry, G. F. Leatherman, D. W. Foster, J. Biol. Chem. **1978**, 253, 4128.
[8] M. E. Franks, G. R. Macpherson, W. D. Figg, Lancet **2004**, 363, 1802.
[9] L. A. Nguyen, H. He, C. Pham-Huy, Int. J. Biomed. Sci. **2006**, 2, 85.
[10] I. Ilisz, A. Aranyi, A. Péter, J. Chromatogr. A **2013**, 1296, 119.
[11] K. A. Schug, W. Lindner, J. Sep. Sci. **2005**, 28, 1932.
[12] Z. Jiang, J. Crassous, V. Schurig, Chirality **2005**, 17, 488.
[13] L. Song, Z. Guo, Y. Chen, Electrophoresis **2012**, 33, 2056.
[14] J. abuta, J. P. Hill, S. Ishihara, L. Hanyková, K. Ariga, Acc. Chem. Res. **2015**, 48, 521.
[15] M. Shahrajabian, F. Ghasemi, M. R. Hormozi-Nezhad, Sci. Rep. **2018**, 8, 14011.
[16] W. Ma, L. Xu, A. F. de Moura, X. Wu, H. Kuang, C. Xu, N. A. Kotov, Chem. Rev. **2017**, 117, 8041.
[17] X. T. Kong, L. V. Besteiro, Z. Wang, A. O. Govorov, Adv. Mater. Interfaces **2018**, e1801790.
[18] A. Cecconello, L. V. Besteiro, A. O. Govorov, I. Willner, Nat. Rev. Mater. **2017**, 2, 17039.
[19] J. T. Collins, C. Kuppe, D. C. Hooper, C. Sibilia, M. Centini, V. K. Valev, Adv. Opt. Mater. **2017**, 5, 1700182.
[20] N. Liu, T. Liedl, Chem. Rev. **2018**, 118, 3032.
[21] M. Qiu, L. Zhang, Z. X. Tang, W. Jin, C. W. Qiu, D. Y. Lei, Adv. Funct. Mater. **2018**, 28, 1803147.
[22] M. Hentschel, M. Schaferling, X. Duan, H. Giessen, N. Liu, Sci. Adv. **2017**, 3, e1602735.
[23] L. D. Barron, *Molecular Light Scattering and Optical Activity*, Cambridge University Press, Cambridge, UK 2004.
[24] B. Nina, N. Koji, R. W. Woody, *Circular Dichroism: Principles and Applications*, John Wiley & Sons, Weinheim, Germany 2000.
[25] N. Amdursky, M. M. Stevens, Chemphyschem **2015**, 16, 2768.
[26] S. A. Maier, *Plasmonics: Fundamentals and Applications*, Springer, New York, US 2007.
[27] W. L. Barnes, A. Dereux, T. W. Ebbesen, Nature **2003**, 424, 824.
[28] N. Yu, F. Capasso, Nat. Mater. **2014**, 13, 139.
[29] J. Mosquera, Y. Zhao, H.-J. Jang, N. Xie, C. Xu, N. A. Kotov, L. M. Liz-Marzán, Adv. Funct. Mater. **2020**, 30, 1902082.
[30] D. K. Gramotnev, S. I. Bozhevolnyi, Nat. Photon. **2010**, 4, 83.
[31] W. Ma, L. Xu, L. Wang, C. Xu, H. Kuang, Adv. Funct. Mater. **2019**, 29, 1805512.
[32] M. J. Urban, C. Shen, X.-T. Kong, C. Zhu, A. O. Govorov, Q. Wang, M. Hentschel, N. Liu, Annu. Rev. Phys. Chem. **2019**, 70, 275.
[33] M. Kuttge, F. J. García de Abajo, A. Polman, Nano Lett. **2010**, 10, 1537.
[34] K. Höflich, R. B. Yang, A. Berger, G. Leuchs, S. Christiansen, Adv. Mater. **2011**, 23, 2657.
[35] J. K. Gansel, M. Thiel, M. S. Rill, M. Decker, K. Bade, V. Saile, G. von Freymann, S. Linden, M. Wegener, Science **2009**, 325, 1513.
[36] S. Mokashi-Punekar, Y. Zhou, S. C. Brooks, N. L. Rosi, Adv. Mater. **2019**, e1905975.
[37] A. O. Govorov, J. Phys. Chem. C **2011**, 115, 7914.
[38] A. O. Govorov, Z. Fan, P. Hernandez, J. M. Slocik, R. R. Naik, Nano Lett. **2010**, 10, 1374.
[39] Z. Y. Bao, J. Dai, Q. Zhang, K. H. Ho, S. Li, C. H. Chan, W. Zhang, D. Y. Lei, Nanoscale **2018**, 10, 19684.
[40] B. Han, Z. Zhu, Z. Li, W. Zhang, Z. Tang, J. Am. Chem. Soc. **2014**, 136, 16104.

[41] W. Ma, C. Hao, M. Sun, L. Xu, C. Xu, H. Kuang, Mater. Horiz. **2018**, 5, 141.
[42] J. Kumar, L. M. Liz-Marzán, Bull. Chem. Soc. Jpn. **2019**, 92, 30.
[43] L. V. Poulikakos, J. A. Dionne, A. García-Etxarri, Symmetry **2019**, 11.
[44] A. Passaseo, M. Esposito, M. Cuscunà, V. Tasco, Adv. Opt. Mater. **2017**, 5, 1601079.
[45] A. Guerrero-Martínez, J. L. Alonso-Gómez, B. Auguié, M. M. Cid, L. M. Liz-Marzán, Nano Today **2011**, 6, 381.
[46] Y. Y. Lee, R. M. Kim, S. W. Im, M. Balamurugan, K. T. Nam, Nanoscale **2020**, 12, 58.
[47] C. Hao, L. Xu, H. Kuang, C. Xu, Adv. Mater. **2019**, e1802075.
[48] T. G. Schaaff, R. L. Whetten, J. Phys. Chem. B **2000**, 104, 2630.
[49] T. G. Schaaff, G. Knight, M. N. Shafigullin, R. F. Borkman, R. L. Whetten, J. Phys. Chem. B **1998**, 102, 10643.
[50] A. Sánchez-Castillo, C. Noguez, I. L. Garzón, J. Am. Chem. Soc. **2010**, 132, 1504.
[51] W. Chen, A. Bian, A. Agarwal, L. Liu, H. Shen, L. Wang, C. Xu, N. A. Kotov, Nano Lett. **2009**, 9, 2153.
[52] J. M. Slocik, A. O. Govorov, R. R. Naik, Nano Lett. **2011**, 11, 701.
[53] Z. Tang, *Chiral Nanomaterials: Preparation, Properties and Applications*, Wiley-VCH, Weinheim, Germany 2018.
[54] A. O. Govorov, Z. Fan, ChemPhysChem **2012**, 13, 2551.
[55] F. Fedorov, Opt. Spectrosc. **1959**, 6, 49.
[56] L. Rosenfeld, Zeitschrift für Physik **1929**, 52, 161.
[57] H. Zhang, A. O. Govorov, Phys. Rev. B **2013**, 87, 075410.
[58] P. Drude, *Lehrbuch der Optik*, S. Hirzel, Leipzig 1900.
[59] M. Born, Phys. Z. **1915**, 16, 251.
[60] B. D. H. Tellegen, Phillips Res. Repts. **1948**, 3, 81.
[61] I. V. Lindell, A. H. Sihvola, S. A. Tretyakov, A. J. Viitanen, *Electromagnetic Waves in Chiral and Bi-Isotropic Media*, Artech House, London 1994.
[62] C. F. Bohren, D. R. Huffman, *Absorption and scattering of light by small particles*, Wiley, Weinheim 1983.
[63] Z. Y. Bao, W. Zhang, Y.-L. Zhang, J. He, J. Dai, C.-T. Yeung, G.-L. Law, D. Y. Lei, Angew. Chem. Int. Ed. **2017**, 56, 1283.
[64] L. Shao, K. C. Woo, H. Chen, Z. Jin, J. Wang, H.-Q. Lin, ACS Nano **2010**, 4, 3053.
[65] L. S. Slaughter, Y. Wu, B. A. Willingham, P. Nordlander, S. Link, ACS Nano **2010**, 4, 4657.
[66] E. Prodan, C. Radloff, N. J. Halas, P. Nordlander, Science **2003**, 302, 419.
[67] B. M. Maoz, R. van der Weegen, Z. Fan, A. O. Govorov, G. Ellestad, N. Berova, E. W. Meijer, G. Markovich, J. Am. Chem. Soc. **2012**, 134, 17807.
[68] K. M. McPeak, C. D. van Engers, S. Bianchi, A. Rossinelli, L. V. Poulikakos, L. Bernard, S. Herrmann, D. K. Kim, S. Burger, M. Blome, S. V. Jayanti, D. J. Norris, Adv. Mater. **2015**, 27, 6244.
[69] W. Liu, Z. Zhu, K. Deng, Z. Li, Y. Zhou, H. Qiu, Y. Gao, S. Che, Z. Tang, J. Am. Chem. Soc. **2013**, 135, 9659.
[70] Z. Zhu, W. Liu, Z. Li, B. Han, Y. Zhou, Y. Gao, Z. Tang, ACS Nano **2012**, 6, 2326.
[71] M. E. Layani, A. Ben Moshe, M. Varenik, O. Regev, H. Zhang, A. O. Govorov, G. Markovich, J. Phys. Chem. C **2013**, 117, 22240.
[72] F. Zhu, X. Li, Y. Li, M. Yan, S. Liu, Anal. Chem. **2015**, 87, 357.
[73] B. Han, L. Shi, X. Gao, J. Guo, K. Hou, Y. Zheng, Z. Tang, Nano Research **2016**, 9, 451.
[74] P. Graf, A. Mantion, A. Haase, A. F. Thünemann, A. Mašić, W. Meier, A. Luch, A. Taubert, ACS Nano **2011**, 5, 820.
[75] J. Lu, Y. X. Chang, N. N. Zhang, Y. Wei, A. J. Li, J. Tai, Y. Xue, Z. Y. Wang, Y. Yang, L. Zhao, Z. Y. Lu, K. Liu, ACS Nano **2017**, 11, 3463.
[76] S. Hou, J. Yan, Z. Hu, X. Wu, Chem. Commun. **2016**, 52, 2059.
[77] X. Lan, Q. Wang, ACS Appl. Mater. Interfaces **2016**, 8, 34598.
[78] S. Abalde-Cela, J. M. Hermida-Ramon, P. Contreras-Carballada, L. De Cola, A. Guerrero-Martinez, R. A. Alvarez-Puebla, L. M. Liz-Marzan, Chemphyschem **2011**, 12, 1529.
[79] B. M. Maoz, Y. Chaikin, A. B. Tesler, O. Bar Elli, Z. Fan, A. O. Govorov, G. Markovich, Nano Lett. **2013**, 13, 1203.

[80] P. Řezanka, K. Záruba, V. Král, Colloids Surf. A Physicochem. Eng. Asp. **2011**, 374, 77.
[81] I. Carmeli, I. Lieberman, L. Kraversky, Z. Fan, A. O. Govorov, G. Markovich, S. Richter, Nano Lett. **2010**, 10, 2069.
[82] N. Hendler, L. Fadeev, E. D. Mentovich, B. Belgorodsky, M. Gozin, S. Richter, Chem. Commun. **2011**, 47, 7419.
[83] G. Shemer, O. Krichevski, G. Markovich, T. Molotsky, I. Lubitz, A. B. Kotlyar, J. Am. Chem. Soc. **2006**, 128, 11006.
[84] X. Lan, X. Zhou, L. A. McCarthy, A. O. Govorov, Y. Liu, S. Link, J. Am. Chem. Soc. **2019**, 141, 19336.
[85] I. Lieberman, G. Shemer, T. Fried, E. M. Kosower, G. Markovich, Angew Chem Int Ed Engl **2008**, 47, 4855.
[86] J.-M. Ha, A. Solovyov, A. Katz, Langmuir **2009**, 25, 153.
[87] A. G. Curto, T. H. Taminiau, G. Volpe, M. P. Kreuzer, R. Quidant, N. F. van Hulst, Nat. Commun. **2013**, 4, 1750.
[88] T. Levi-Belenkova, A. O. Govorov, G. Markovich, J. Phys. Chem. C **2016**, 120, 12751.
[89] F. Lu, Y. Tian, M. Liu, D. Su, H. Zhang, A. O. Govorov, O. Gang, Nano Lett. **2013**, 13, 3145.
[90] S. Huang, T. Ming, Y. Lin, X. Ling, Q. Ruan, T. Palacios, J. Wang, M. Dresselhaus, J. Kong, Small **2016**, 12, 5190.
[91] W. Zhu, M. G. Banaee, D. Wang, Y. Chu, K. B. Crozier, Small **2011**, 7, 1761.
[92] W. Zhu, K. B. Crozier, Nat. Commun. **2014**, 5, 5228.
[93] X. Wu, P. Fu, W. Ma, L. Xu, H. Kuang, C. Xu, RSC Adv. **2015**, 5, 73395.
[94] G. M. Akselrod, C. Argyropoulos, T. B. Hoang, C. Ciraci, C. Fang, J. N. Huang, D. R. Smith, M. H. Mikkelsen, Nat. Photon. **2014**, 8, 835.
[95] B. Gerislioglu, L. Dong, A. Ahmadivand, H. Hu, P. Nordlander, N. J. Halas, Nano Lett. **2020**, 20, 2087.
[96] R. M. Ma, S. Ota, Y. Li, S. Yang, X. Zhang, Nat. Nanotechnol. **2014**, 9, 600.
[97] R.-Y. Wang, P. Wang, Y. Liu, W. Zhao, D. Zhai, X. Hong, Y. Ji, X. Wu, F. Wang, D. Zhang, W. Zhang, R. Liu, X. Zhang, J. Phys. Chem. C **2014**, 118, 9690.
[98] H. Chen, L. Shao, Q. Li, J. Wang, Chem Soc Rev **2013**, 42, 2679.
[99] P. K. Jain, S. Eustis, M. A. El-Sayed, J. Phys. Chem. B **2006**, 110, 18243.
[100] Z. Li, Z. Zhu, W. Liu, Y. Zhou, B. Han, Y. Gao, Z. Tang, J. Am. Chem. Soc. **2012**, 134, 3322.
[101] L. Chang, Y. Khan, L. Li, N. Yang, P. Yin, L. Guo, RSC Adv. **2017**, 7, 13896.
[102] L. M. Kneer, E.-M. Roller, L. V. Besteiro, R. Schreiber, A. O. Govorov, T. Liedl, ACS Nano **2018**, 12, 9110.
[103] P. Gu, T. Zheng, W. Zhang, B. Ai, Z. Zhao, G. Zhang, Adv. Mater. Interfaces **2020**, 7, 1902021.
[104] C. Hao, L. Xu, W. Ma, L. Wang, H. Kuang, C. Xu, Small **2014**, 10, 1805.
[105] Y. Zhao, L. Xu, W. Ma, L. Wang, H. Kuang, C. Xu, N. A. Kotov, Nano Lett. **2014**, 14, 3908.
[106] R. Ghosh Chaudhuri, S. Paria, Chem. Rev. **2012**, 112, 2373.
[107] M. B. Gawande, A. Goswami, T. Asefa, H. Guo, A. V. Biradar, D.-L. Peng, R. Zboril, R. S. Varma, Chem. Soc. Rev. **2015**, 44, 7540.
[108] O. Peña-Rodríguez, U. Pal, Nanoscale Res. Lett. **2011**, 6, 279.
[109] D. J. Wu, X. J. Liu, Appl. Phys. B **2009**, 97, 193.
[110] O. Peña-Rodríguez, U. Pal, Nanoscale **2011**, 3, 3609.
[111] R. Bardhan, S. Mukherjee, N. A. Mirin, S. D. Levit, P. Nordlander, N. J. Halas, J. Phys. Chem. C **2010**, 114, 7378.
[112] C. Hao, L. Xu, W. Ma, X. Wu, L. Wang, H. Kuang, C. Xu, Adv. Funct. Mater. **2015**, 25, 5816.
[113] C. Hao, L. Xu, M. Sun, W. Ma, H. Kuang, C. Xu, Adv. Funct. Mater. **2018**, 28.
[114] X. Wu, L. Xu, W. Ma, L. Liu, H. Kuang, W. Yan, L. Wang, C. Xu, Adv. Funct. Mater. **2015**, 25, 850.
[115] J. Yan, Y. Chen, S. Hou, J. Chen, D. Meng, H. Zhang, H. Fan, Y. Ji, X. Wu, Nanoscale **2017**, 9, 11093.
[116] G. Zheng, Z. Bao, J. Perez-Juste, R. Du, W. Liu, J. Dai, W. Zhang, L. Y. S. Lee, K. Y. Wong, Angew Chem Int Ed Engl **2018**, 57, 16452.
[117] N. A. Abdulrahman, Z. Fan, T. Tonooka, S. M. Kelly, N. Gadegaard, E. Hendry, A. O. Govorov, M. Kadodwala, Nano Lett. **2012**, 12, 977.
[118] S. Ostovar pour, L. Rocks, K. Faulds, D. Graham, V. Parchansky, P. Bour, E. W. Blanch, Nat. Chem. **2015**, 7, 591.

[119] L. Verslegers, Z. Yu, Z. Ruan, P. B. Catrysse, S. Fan, Phys. Rev. Lett. **2012**, 108, 083902.
[120] J. Wiersig, Phys. Rev. Lett. **2006**, 97, 253901.
[121] L. Hu, T. Liedl, K. Martens, Z. Wang, A. O. Govorov, ACS Photonics **2019**, 6, 749.
[122] A. Guerrero-Martínez, M. Grzelczak, L. M. Liz-Marzán, ACS Nano **2012**, 6, 3655.
[123] Z. Fan, A. O. Govorov, Nano Lett. **2010**, 10, 2580.
[124] Z. Fan, A. O. Govorov, J. Phys. Chem. C **2011**, 115, 13254.
[125] Z. Fan, H. Zhang, A. O. Govorov, J. Phys. Chem. C **2013**, 117, 14770.
[126] V. E. Ferry, J. M. Smith, A. P. Alivisatos, ACS Photonics **2014**, 1, 1189.
[127] Z. Fan, A. O. Govorov, Nano Lett. **2012**, 12, 3283.
[128] I. Dolamic, S. Knoppe, A. Dass, T. Burgi, Nat. Commun. **2012**, 3, 798.
[129] S. Liu, L. Han, Y. Duan, S. Asahina, O. Terasaki, Y. Cao, B. Liu, L. Ma, J. Zhang, S. Che, Nat. Commun. **2012**, 3, 1215.
[130] A. Ben-Moshe, S. G. Wolf, M. Bar Sadan, L. Houben, Z. Fan, A. O. Govorov, G. Markovich, Nat. Commun. **2014**, 5, 4302.
[131] J. Yeom, B. Yeom, H. Chan, K. W. Smith, S. Dominguez-Medina, Joong H. Bahng, G. Zhao, W.-S. Chang, S.-J. Chang, A. Chuvilin, D. Melnikau, A. L. Rogach, P. Zhang, S. Link, P. Král, N. A. Kotov, Nat. Mater. **2015**, 14, 66.
[132] Y. Kim, B. Yeom, O. Arteaga, S. Jo Yoo, S.-G. Lee, J.-G. Kim, N. A. Kotov, Nat. Mater. **2016**, 15, 461.
[133] A. Guerrero-Martínez, B. Auguié, J. L. Alonso-Gómez, Z. Džolić, S. Gómez-Graña, M. Žinić, M. M. Cid, L. M. Liz-Marzán, Angew. Chem. Int. Ed. **2011**, 50, 5499.
[134] H. S. Oh, S. Liu, H. Jee, A. Baev, M. T. Swihart, P. N. Prasad, J. Am. Chem. Soc. **2010**, 132, 17346.
[135] C.-L. Chen, P. Zhang, N. L. Rosi, J. Am. Chem. Soc. **2008**, 130, 13555.
[136] C.-L. Chen, N. L. Rosi, J. Am. Chem. Soc. **2010**, 132, 6902.
[137] C. Song, M. G. Blaber, G. Zhao, P. Zhang, H. C. Fry, G. C. Schatz, N. L. Rosi, Nano Lett. **2013**, 13, 3256.
[138] C. Zhang, C. Song, H. C. Fry, N. L. Rosi, Chem. Eur. J. **2014**, 20, 941.
[139] A. D. Merg, J. Slocik, M. G. Blaber, G. C. Schatz, R. Naik, N. L. Rosi, Langmuir **2015**, 31, 9492.
[140] A. D. Merg, J. C. Boatz, A. Mandal, G. Zhao, S. Mokashi-Punekar, C. Liu, X. Wang, P. Zhang, P. C. A. van der Wel, N. L. Rosi, J. Am. Chem. Soc. **2016**, 138, 13655.
[141] Y. Lin, E. T. Pashuck, M. R. Thomas, N. Amdursky, S. T. Wang, L. W. Chow, M. M. Stevens, Angew Chem Int Ed Engl **2017**, 56, 2361.
[142] Y. Li, M. Liu, Chem. Commun. **2008**, 5571.
[143] L. Zhu, X. Li, S. Wu, K. T. Nguyen, H. Yan, H. Ågren, Y. Zhao, J. Am. Chem. Soc. **2013**, 135, 9174.
[144] S. H. Jung, J. Jeon, H. Kim, J. Jaworski, J. H. Jung, J. Am. Chem. Soc. **2014**, 136, 6446.
[145] H. Qi, K. E. Shopsowitz, W. Y. Hamad, M. J. MacLachlan, J. Am. Chem. Soc. **2011**, 133, 3728.
[146] A. Querejeta-Fernández, G. Chauve, M. Methot, J. Bouchard, E. Kumacheva, J. Am. Chem. Soc. **2014**, 136, 4788.
[147] G. Chu, X. Wang, T. Chen, J. Gao, F. Gai, Y. Wang, Y. Xu, ACS Appl. Mater. Interfaces **2015**, 7, 11863.
[148] A. Querejeta-Fernández, B. Kopera, K. S. Prado, A. Klinkova, M. Methot, G. Chauve, J. Bouchard, A. S. Helmy, E. Kumacheva, ACS Nano **2015**, 9, 10377.
[149] D. Qu, J. Zhang, G. Chu, H. Jiang, C. Wu, Y. Xu, Journal of Materials Chemistry C **2016**, 4, 1764.
[150] S. Che, Z. Liu, T. Ohsuna, K. Sakamoto, O. Terasaki, T. Tatsumi, Nature **2004**, 429, 281.
[151] H. Qiu, S. Che, Chem. Soc. Rev. **2011**, 40, 1259.
[152] J. Xie, S. Che, Chem. Eur. J. **2012**, 18, 15954.
[153] J. Xie, Y. Duan, S. Che, Adv. Funct. Mater. **2012**, 22, 3784.
[154] X. Fu, Y. Wang, L. Huang, Y. Sha, L. Gui, L. Lai, Y. Tang, Adv. Mater. **2003**, 15, 902.
[155] G. A. Silva, C. Czeisler, K. L. Niece, E. Beniash, D. A. Harrington, J. A. Kessler, S. I. Stupp, Science **2004**, 303, 1352.
[156] G. Chu, X. Wang, H. Yin, Y. Shi, H. Jiang, T. Chen, J. Gao, D. Qu, Y. Xu, D. Ding, ACS Appl. Mater. Interfaces **2015**, 7, 21797.
[157] A. Lukach, H. Thérien-Aubin, A. Querejeta-Fernández, N. Pitch, G. Chauve, M. Méthot, J. Bouchard, E. Kumacheva, Langmuir **2015**, 31, 5033.
[158] B. Vollick, P.-Y. Kuo, H. Thérien-Aubin, N. Yan, E. Kumacheva, Chemistry of Materials **2017**, 29, 789.
[159] B. Ding, Z. Deng, H. Yan, S. Cabrini, R. N. Zuckermann, J. Bokor, J. Am. Chem. Soc. **2010**, 132, 3248.

[160] T. Molotsky, T. Tamarin, A. B. Moshe, G. Markovich, A. B. Kotlyar, J. Phys. Chem. C **2010**, 114, 15951.
[161] A. P. Alivisatos, K. P. Johnsson, X. Peng, T. E. Wilson, C. J. Loweth, M. P. Bruchez, P. G. Schultz, Nature **1996**, 382, 609.
[162] J. Sharma, R. Chhabra, A. Cheng, J. Brownell, Y. Liu, H. Yan, Science **2009**, 323, 112.
[163] S. M. Douglas, H. Dietz, T. Liedl, B. Högberg, F. Graf, W. M. Shih, Nature **2009**, 459, 414.
[164] A. J. Mastroianni, S. A. Claridge, A. P. Alivisatos, J. Am. Chem. Soc. **2009**, 131, 8455.
[165] W. Yan, L. Xu, C. Xu, W. Ma, H. Kuang, L. Wang, N. A. Kotov, J. Am. Chem. Soc. **2012**, 134, 15114.
[166] X. Wu, L. Xu, W. Ma, L. Liu, H. Kuang, N. A. Kotov, C. Xu, Adv. Mater. **2016**, 28, 5907.
[167] P. W. K. Rothemund, Nature **2006**, 440, 297.
[168] A. M. Maier, W. Bae, D. Schiffels, J. F. Emmerig, M. Schiff, T. Liedl, ACS Nano **2017**, 11, 1301.
[169] A. Kuzyk, R. Schreiber, Z. Fan, G. Pardatscher, E. M. Roller, A. Hogele, F. C. Simmel, A. O. Govorov, T. Liedl, Nature **2012**, 483, 311.
[170] X. Shen, A. Asenjo-Garcia, Q. Liu, Q. Jiang, F. J. García de Abajo, N. Liu, B. Ding, Nano Lett. **2013**, 13, 2128.
[171] M. J. Urban, P. K. Dutta, P. Wang, X. Duan, X. Shen, B. Ding, Y. Ke, N. Liu, J. Am. Chem. Soc. **2016**, 138, 5495.
[172] T. G. W. Edwardson, K. L. Lau, D. Bousmail, C. J. Serpell, H. F. Sleiman, Nat. Chem. **2016**, 8, 162.
[173] Y. Tian, T. Wang, W. Liu, H. L. Xin, H. Li, Y. Ke, W. M. Shih, O. Gang, Nat. Nanotechnol. **2015**, 10, 637.
[174] G. Dai, X. Lu, Z. Chen, C. Meng, W. Ni, Q. Wang, ACS Appl. Mater. Interfaces **2014**, 6, 5388.
[175] T. Liu, L. V. Besteiro, T. Liedl, M. A. Correa-Duarte, Z. Wang, A. O. Govorov, Nano Lett. **2019**, 19, 1395.
[176] X. Lan, Z. Chen, G. Dai, X. Lu, W. Ni, Q. Wang, J. Am. Chem. Soc. **2013**, 135, 11441.
[177] F. Neubrech, M. Hentschel, N. Liu, Adv. Mater. **2020**, e1905640.
[178] M.-K. Nguyen, A. Kuzyk, ACS Nano **2019**, 13, 13615.
[179] R. Schreiber, N. Luong, Z. Fan, A. Kuzyk, P. C. Nickels, T. Zhang, D. M. Smith, B. Yurke, W. Kuang, A. O. Govorov, T. Liedl, Nat. Commun. **2013**, 4, 2948.
[180] A. Kuzyk, R. Schreiber, H. Zhang, A. O. Govorov, T. Liedl, N. Liu, Nat. Mater. **2014**, 13, 862.
[181] X. Lan, T. Liu, Z. Wang, A. O. Govorov, H. Yan, Y. Liu, J. Am. Chem. Soc. **2018**, 140, 11763.
[182] M. Wang, J. Dong, C. Zhou, H. Xie, W. Ni, S. Wang, H. Jin, Q. Wang, ACS Nano **2019**, 13, 13702.
[183] Y. Zhou, R. L. Marson, G. van Anders, J. Zhu, G. Ma, P. Ercius, K. Sun, B. Yeom, S. C. Glotzer, N. A. Kotov, ACS Nano **2016**, 10, 3248.
[184] H.-E. Lee, J. Lee, M. Ju, H.-Y. Ahn, Y. Y. Lee, H.-S. Jang, K. T. Nam, Mol. Syst. Des. Eng. **2018**, 3, 581.
[185] W. Xiao, K.-H. Ernst, K. Palotas, Y. Zhang, E. Bruyer, L. Peng, T. Greber, W. A. Hofer, L. T. Scott, R. Fasel, Nat. Chem. **2016**, 8, 326.
[186] H. E. Lee, H. Y. Ahn, J. Mun, Y. Y. Lee, M. Kim, N. H. Cho, K. Chang, W. S. Kim, J. Rho, K. T. Nam, Nature **2018**, 556, 360.
[187] A. Ben-Moshe, A. O. Govorov, G. Markovich, Angew. Chem. Int. Ed. **2013**, 52, 1275.
[188] S.-T. Wang, Y. Lin, N. Todorova, Y. Xu, M. Mazo, S. Rana, V. Leonardo, N. Amdursky, C. D. Spicer, B. D. Alexander, A. A. Edwards, S. J. Matthews, I. Yarovsky, M. M. Stevens, Chemistry of Materials **2017**, 29, 1550.
[189] H. Liu, Y. Ye, J. Chen, D. Lin, Z. Jiang, Z. Liu, B. Sun, L. Yang, J. Liu, Chem. Eur. J. **2012**, 18, 8037.
[190] T. Li, H. G. Park, H.-S. Lee, S.-H. Choi, Nanotechnology **2004**, 15, S660.
[191] C. Li, K. Deng, Z. Tang, L. Jiang, J. Am. Chem. Soc. **2010**, 132, 8202.
[192] J.-S. Shen, D.-H. Li, M.-B. Zhang, J. Zhou, H. Zhang, Y.-B. Jiang, Langmuir **2011**, 27, 481.
[193] M. C. di Gregorio, A. Ben Moshe, E. Tirosh, L. Galantini, G. Markovich, J. Phys. Chem. C **2015**, 119, 17111.
[194] G. G. Huang, X. X. Han, M. K. Hossain, Y. Kitahama, Y. Ozaki, Appl. Spectmsc. **2010**, 64, 1100.
[195] A. Ben-Moshe, B. M. Maoz, A. O. Govorov, G. Markovich, Chem. Soc. Rev. **2013**, 42, 7028.
[196] Y. Huang, M. K. Nguyen, A. K. Natarajan, V. H. Nguyen, A. Kuzyk, ACS Appl Mater Interfaces **2018**, 10, 44221.
[197] T. Funck, F. Nicoli, A. Kuzyk, T. Liedl, Angew. Chem. Int. Ed. **2018**, 57, 13495.
[198] L. Xu, Z. Xu, W. Ma, L. Liu, L. Wang, H. Kuang, C. Xu, J. Mater. Chem. B **2013**, 1, 4478.
[199] J. Wang, S.-S. Zhang, X. Xu, K.-X. Fei, Y.-X. Peng, Nanomaterials **2018**, 8, 1027.
[200] W. Ma, H. Kuang, L. Xu, L. Ding, C. Xu, L. Wang, N. A. Kotov, Nat. Commun. **2013**, 4, 2689.

[201] X. Wu, L. Xu, L. Liu, W. Ma, H. Yin, H. Kuang, L. Wang, C. Xu, N. A. Kotov, J. Am. Chem. Soc. **2013**, 135, 18629.
[202] B. Auguié, J. L. Alonso-Gómez, A. Guerrero-Martínez, L. M. Liz-Marzán, J. Phys. Chem. Lett. **2011**, 2, 846.
[203] M. Sun, L. Xu, J. H. Bahng, H. Kuang, S. Alben, N. A. Kotov, C. Xu, Nat. Commun. **2017**, 8, 1847.
[204] L. Xu, Y. Gao, H. Kuang, L. M. Liz-Marzan, C. Xu, Angew Chem Int Ed Engl **2018**, 57, 10544.
[205] W. Yan, Y. Wang, H. Zhuang, J. Zhang, Biosens. Bioelectron. **2015**, 68, 516.
[206] F. Gao, M. Sun, W. Ma, X. Wu, L. Liu, H. Kuang, C. Xu, Adv. Mater. **2017**, 29, 1606864.
[207] S. Li, L. Xu, W. Ma, X. Wu, M. Sun, H. Kuang, L. Wang, N. A. Kotov, C. Xu, J. Am. Chem. Soc. **2016**, 138, 306.
[208] M. Sun, A. Qu, C. Hao, X. Wu, L. Xu, C. Xu, H. Kuang, Adv. Mater. **2018**, 30, 1804241.
[209] L. V. Besteiro, H. Zhang, J. Plain, G. Markovich, Z. Wang, A. O. Govorov, Adv. Opt. Mater. **2017**, 5, 1700069.
[210] Q. Zhang, T. Hernandez, K. W. Smith, S. A. Hosseini Jebeli, A. X. Dai, L. Warning, R. Baiyasi, L. A. McCarthy, H. Guo, D.-H. Chen, J. A. Dionne, C. F. Landes, S. Link, Science **2019**, 365, 1475.
[211] J.-Y. Kim, N. A. Kotov, Science **2019**, 365, 1378.
[212] W. Ma, H. Kuang, L. Wang, L. Xu, W.-S. Chang, H. Zhang, M. Sun, Y. Zhu, Y. Zhao, L. Liu, C. Xu, S. Link, N. A. Kotov, Sci. Rep. **2013**, 3, 1934.
[213] K. W. Smith, H. Zhao, H. Zhang, A. Sanchez-Iglesias, M. Grzelczak, Y. Wang, W. S. Chang, P. Nordlander, L. M. Liz-Marzan, S. Link, ACS Nano **2016**, 10, 6180.
[214] T. Wu, J. Ren, R. Wang, X. Zhang, J. Phys. Chem. C **2014**, 118, 20529.
[215] S. Yang, Z. Liu, S. Hu, A. Z. Jin, H. Yang, S. Zhang, J. Li, C. Gu, Nano Lett. **2019**, 19, 3432.
[216] B. Semnani, J. Flannery, R. Al Maruf, M. Bajcsy, Light: Science & Applications **2020**, 9, 23.
[217] J. Kumar, H. Eraña, E. López-Martínez, N. Claes, V. F. Martín, D. M. Solís, S. Bals, A. L. Cortajarena, J. Castilla, L. M. Liz-Marzán, Proceedings of the National Academy of Sciences **2018**, 115, 3225.
[218] S. Abbasi, H. Khani, Spectrochimica Acta Part A: Molecular and Biomolecular Spectroscopy **2017**, 186, 76.
[219] Y. Zhu, L. Xu, W. Ma, Z. Xu, H. Kuang, L. Wang, C. Xu, Chem. Commun. **2012**, 48, 11889.
[220] Z. Xu, L. Xu, L. M. Liz-Marzán, W. Ma, N. A. Kotov, L. Wang, H. Kuang, C. Xu, Adv. Opt. Mater. **2013**, 1, 626.
[221] M. Sun, L. Xu, P. Fu, X. Wu, H. Kuang, L. Liu, C. Xu, Adv. Funct. Mater. **2016**, 26, 7352.

Figures:

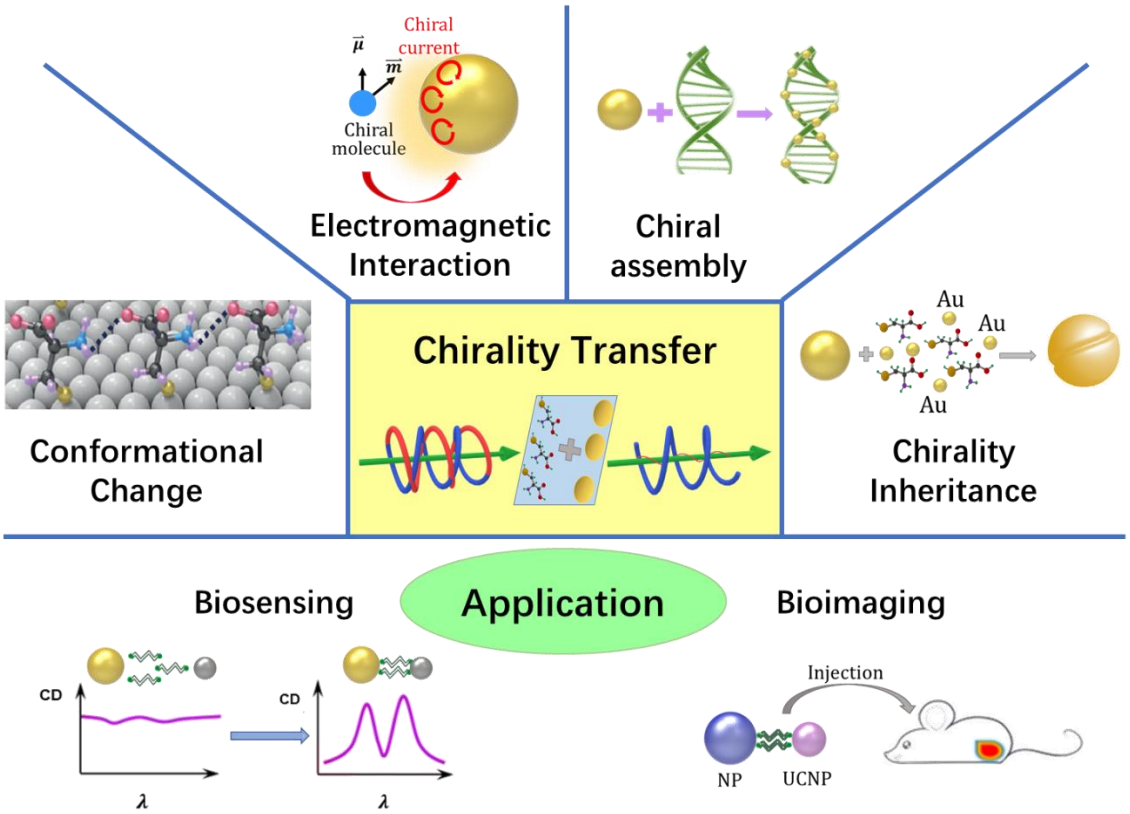

Scheme 1. Schematic illustration of the mechanisms and applications of chirality transfer. Copyright 2012, American Chemical Society. Reproduced with permission.[63]

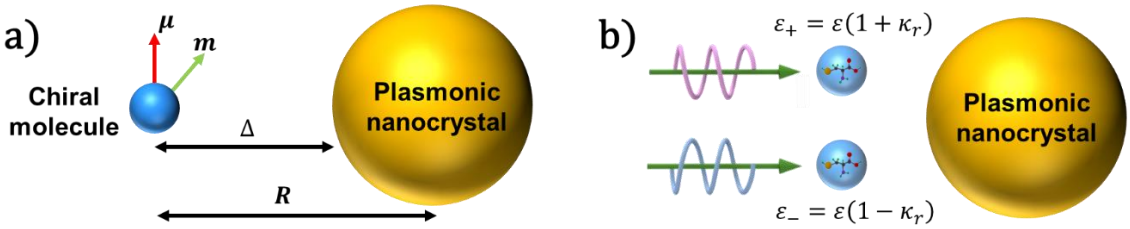

Figure 1. (a) Mechanism illustration of the density-matrix formalism. (b) Mechanism illustration of effective polarizability.

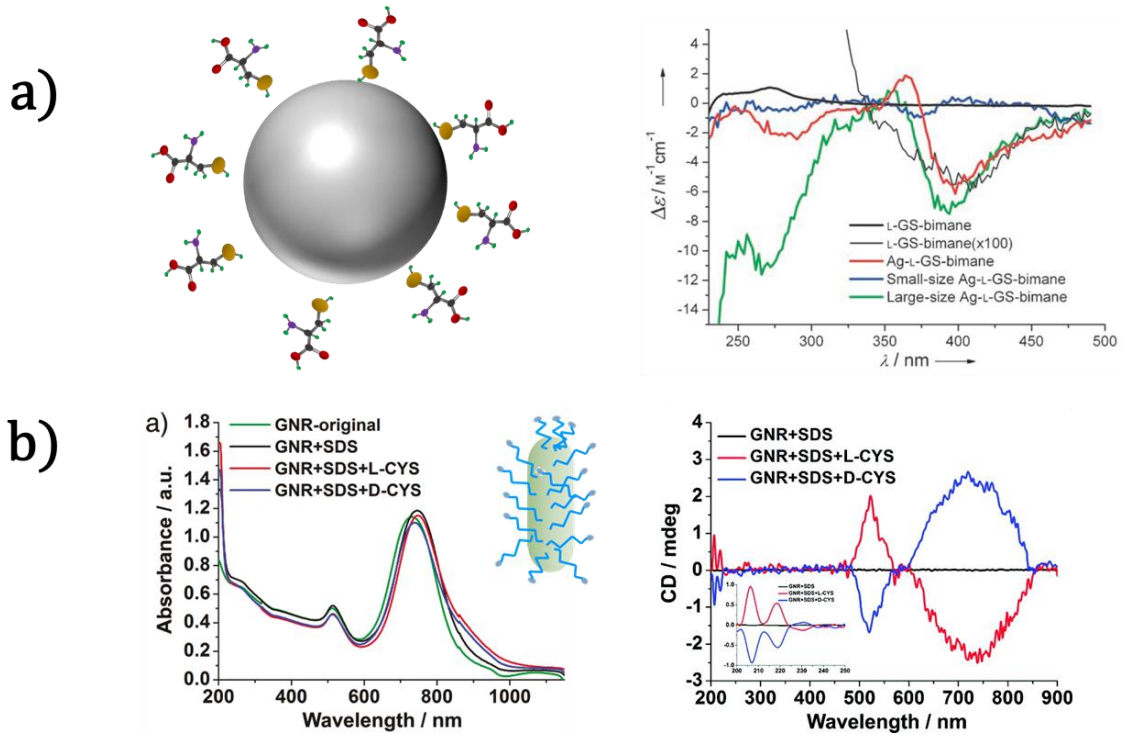

Figure 2. (a) Schematic illustration of Ag NPs coated with chiral molecules (left) and its corresponding CD spectra (right).[85] (b) The absorption (left) and CD spectra (right) of Au NRs coated with Cys molecules.[70] (a) Reproduced with permission.[85] Copyright 2008, Wiley. (b) Reproduced with permission.[70] Copyright 2012, American Chemical Society.

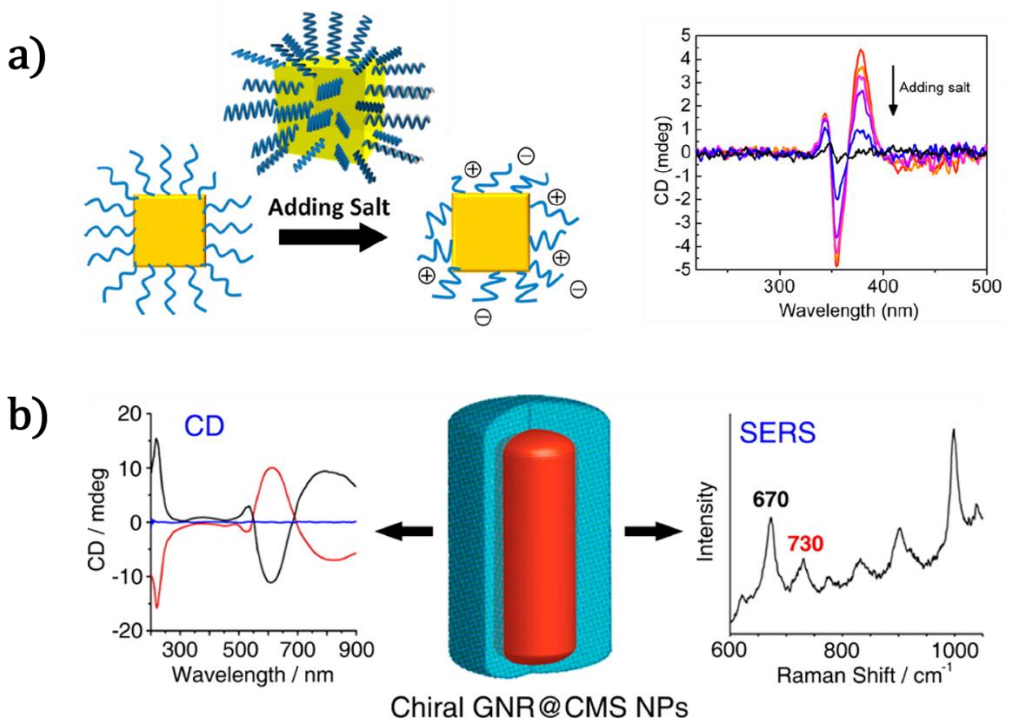

Figure 3. Schematic illustration of gold/silver core/shell NC synthesis (left) and CD response and absorption spectra of ssDNA-coated Ag NCs (right).[89] (b) CD and SERS

spectra of chiral AuNR@CMS NPs.[69] (a) Reproduced with permission.[89] Copyright 2013, American Chemical Society. (b) Reproduced with permission.[69] Copyright 2013, American Chemical Society.

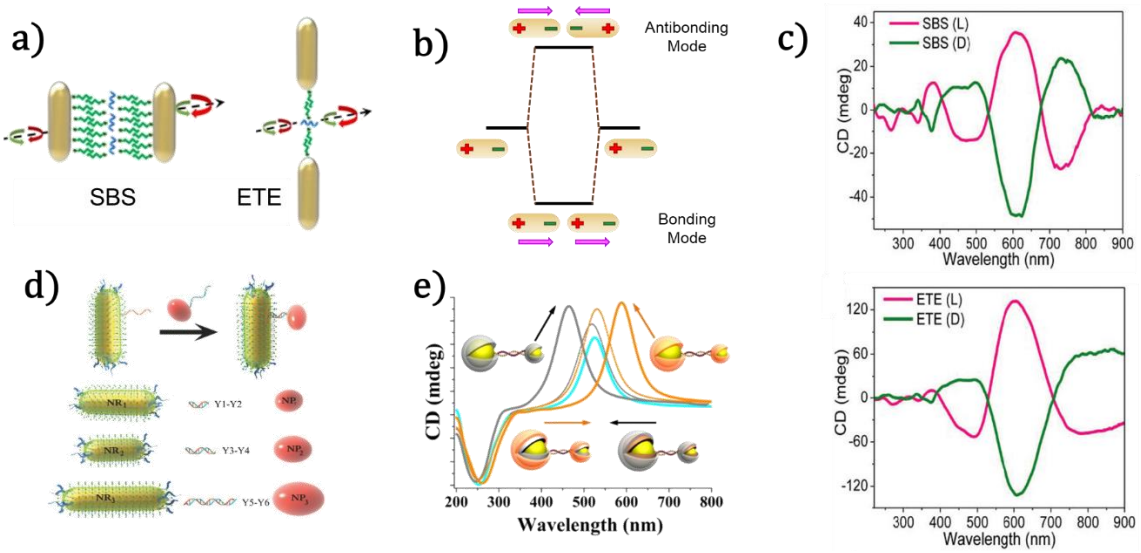

Figure 4. (a) Schematic illustration of Au NRs with SBS (left) and ETE (right) configurations. (b) Model of coupled longitudinal plasmon excitation in the ETE Au NRs configuration (c) Chiroptical responses from Au@Ag SBS (top) and Au@Ag ETE (bottom) configurations.[39] (d) Schematic illustration of Au NP-NR heterodimers connected by DNA with different lengths.[104] (e) Chiroptical response of Au/Ag (or Au/Au) core/shell heterodimers linked by DNA.[105] (a) (c) Reproduced with permission.[39] Copyright 2018, The Royal Society of Chemistry. (d) Reproduced with permission.[104] Copyright 2014, Wiley. (e) Reproduced with permission.[105] Copyright 2014, American Chemical Society.

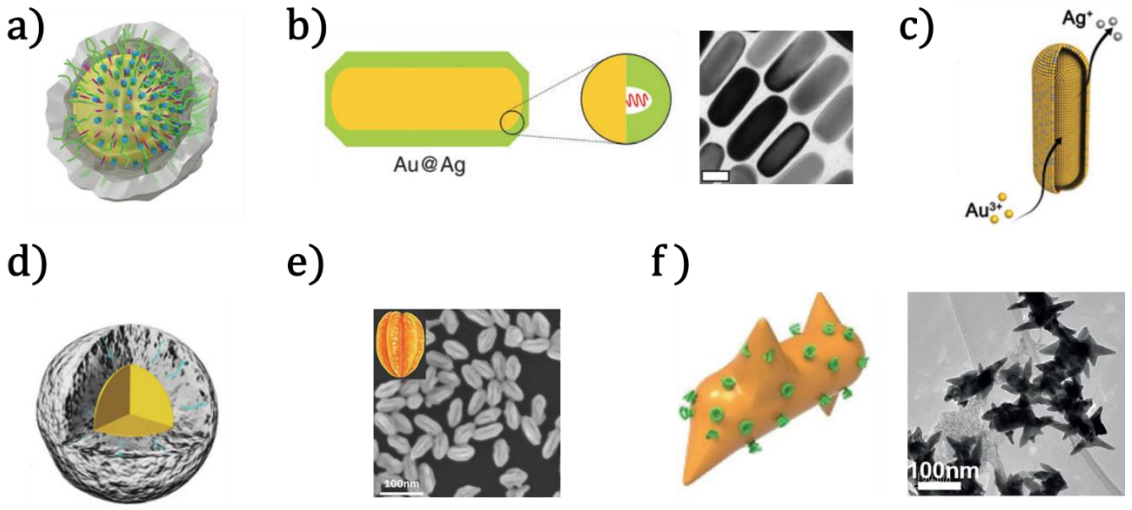

Figure 5. Typical core-shell structures with enhanced fields. (a) Gold-gap-silver core-shell nanoparticles with nanogap filled with Cys.[112] (b) Au-cysteine-Ag core-shell nanorod.[76] (c) Au@AgAu yolk–shell nanorods.[113] (d) Au core–DNA–Ag shell quasi-spherical nanoparticles.[114] (e) Starfruit-like Au@Ag NPs.[115] (f) Au NRs with sharp spikes.[116] (a)

Reproduced with permission.[112] Copyright 2015, Wiley. (b) Reproduced with permission.[76] Copyright 2016, The Royal Society of Chemistry. (c) Reproduced with permission.[113] Copyright 2015, Wiley. (d) Reproduced with permission.[114] Copyright 2015, Wiley. (e) Reproduced with permission.[115] Copyright 2017, The Royal Society of Chemistry. (f) Reproduced with permission.[116] Copyright 2018, Wiley.

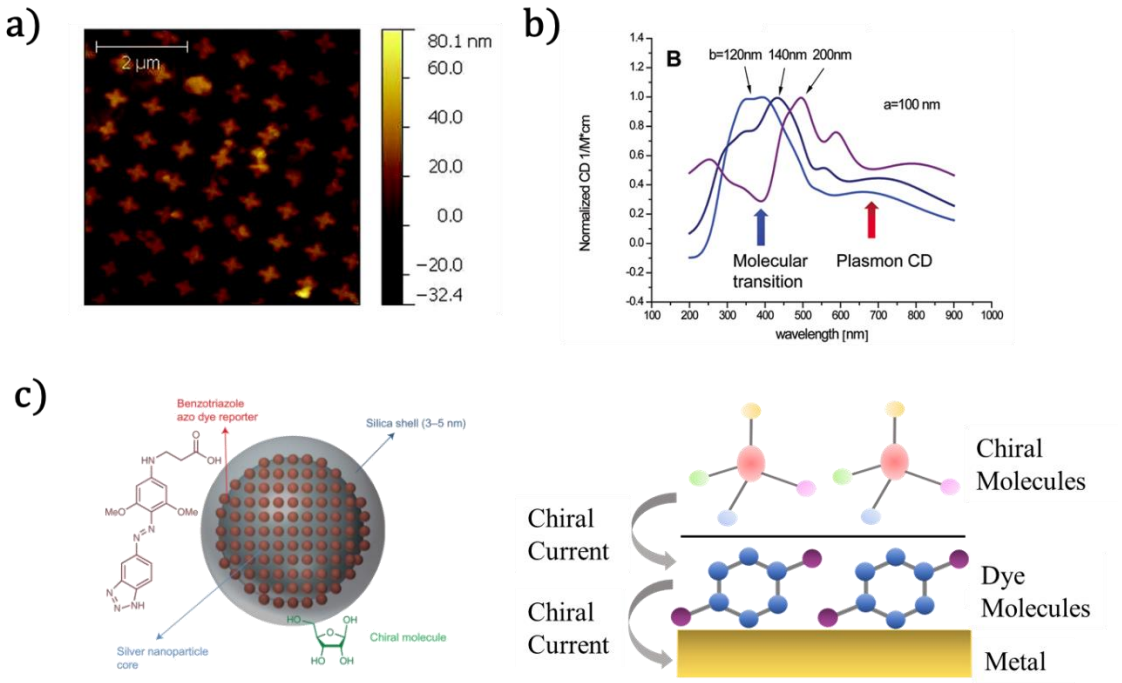

Figure 6. (a) Gold cross substrate used for long-range electromagnetic interaction.[117] (b) Calculated CD spectra of the hybrid gold core−chiral shell structures with shell thickness b = 120, 140, 200 nm.[117] (c) Left: schematic of a silver nanotag coated with chiral molecules.[118] Right: mechanism of through-space chirality transfer. (a) (b) Reproduced with permission.[117] Copyright 2012, American Chemical Society. (c) Reproduced with permission.[118] Copyright 2015, Springer Nature.

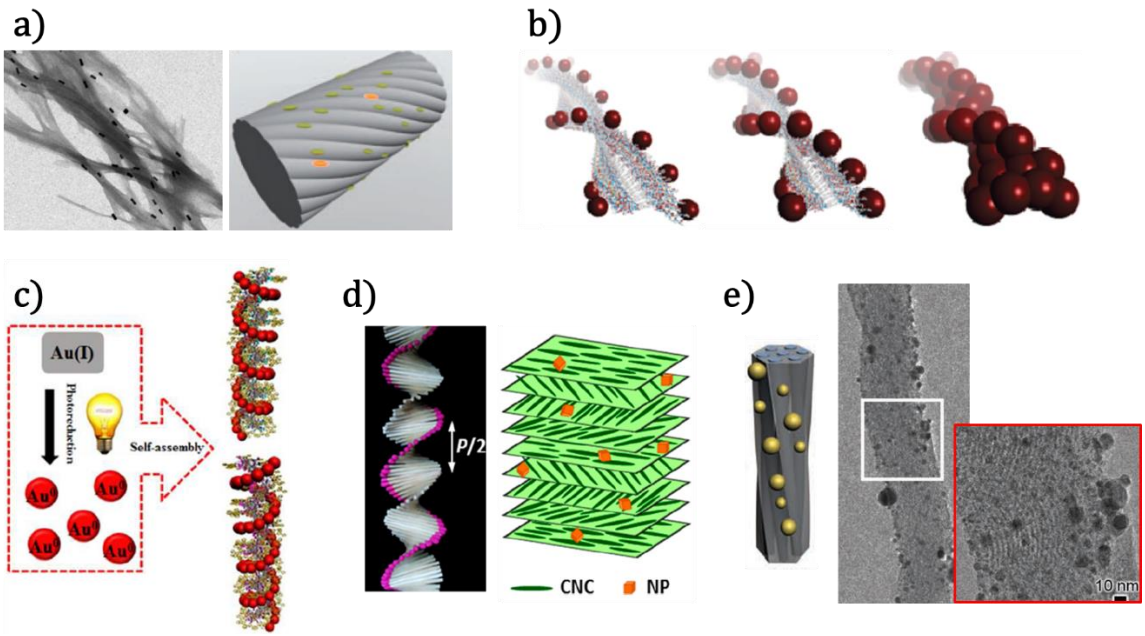

Figure 7. Typical chiral template for assembling chiral plasmonic superstructures. (a) Gold NRs adsorbed on twisted fibers template.[133] (b) Various tailorable peptide-patterned nanoparticle superstructures with different NP radius.[136] (c) Assembly procedure of organogelators guided Au NRs superstructures.[144] (d) Schematics of Au NPs loaded on chiral CNC films.[148] (e) Schematics and TEM image of Ag-CMS-as superstructures.[153] (a) Reproduced with permission.[133] Copyright 2011, Wiley. (b) Reproduced with permission.[136] Copyright 2010, American Chemical Society. (c) Reproduced with permission.[144] Copyright 2014, American Chemical Society. (d) Reproduced with permission.[148] Copyright 2015, American Chemical Society. (e) Reproduced with permission.[153] Copyright 2012, Wiley.

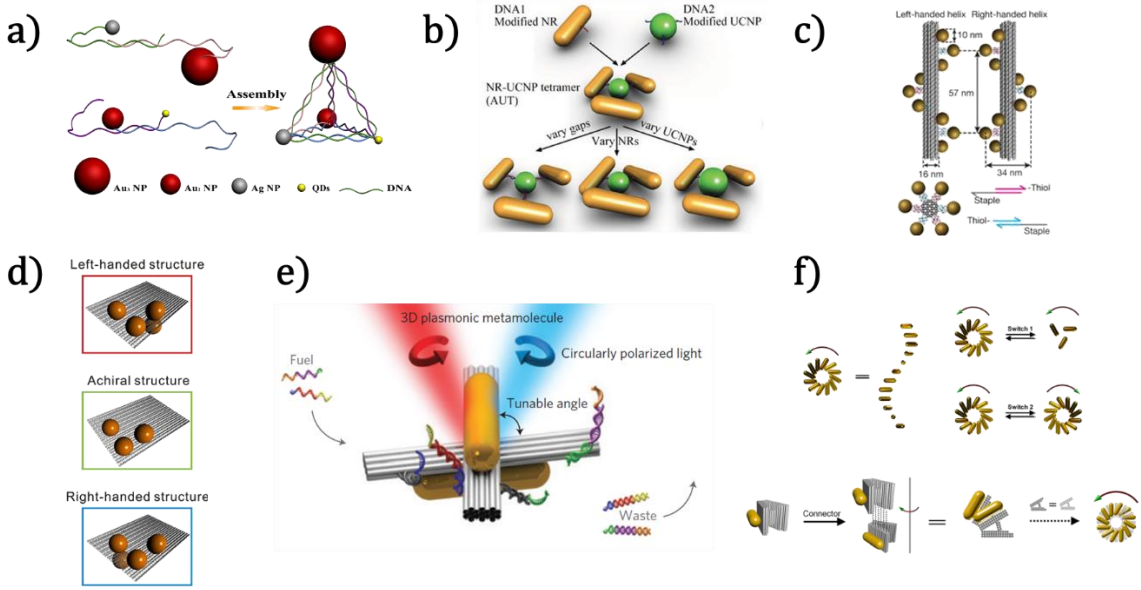

Figure 8. (a) Schematic of a chiral NPs pyramid composed of two Au NPs, one Ag NPs

and a QD.[165] (b) Schematic of the Au NR-UCNP tetramer assemblies.[166] (c) Schematic illustration of the principle of self-assembly and structural reconfiguration (top and side view) of the chiral plasmonic superstructures of Au NR.[169] (d) Right- and left- handed plasmonic tetramer created by a rectangular DNA template.[170] (e) Plamsonic cross loaded on DNA origami.[180] (f) Asymmetric Au helices on a DNA bundle origami structure.[181] (a) Reproduced with permission.[165] Copyright 2012, American Chemical Society. (b) Reproduced with permission.[166] Copyright 2016, Wiley. (c) Reproduced with permission.[169] Copyright 2012, Springer Nature. (d) Reproduced with permission.[170] Copyright 2013, American Chemical Society. (e) Reproduced with permission.[180] Copyright 2014, Springer Nature. (f) Reproduced with permission.[181] Copyright 2018, American Chemical Society.

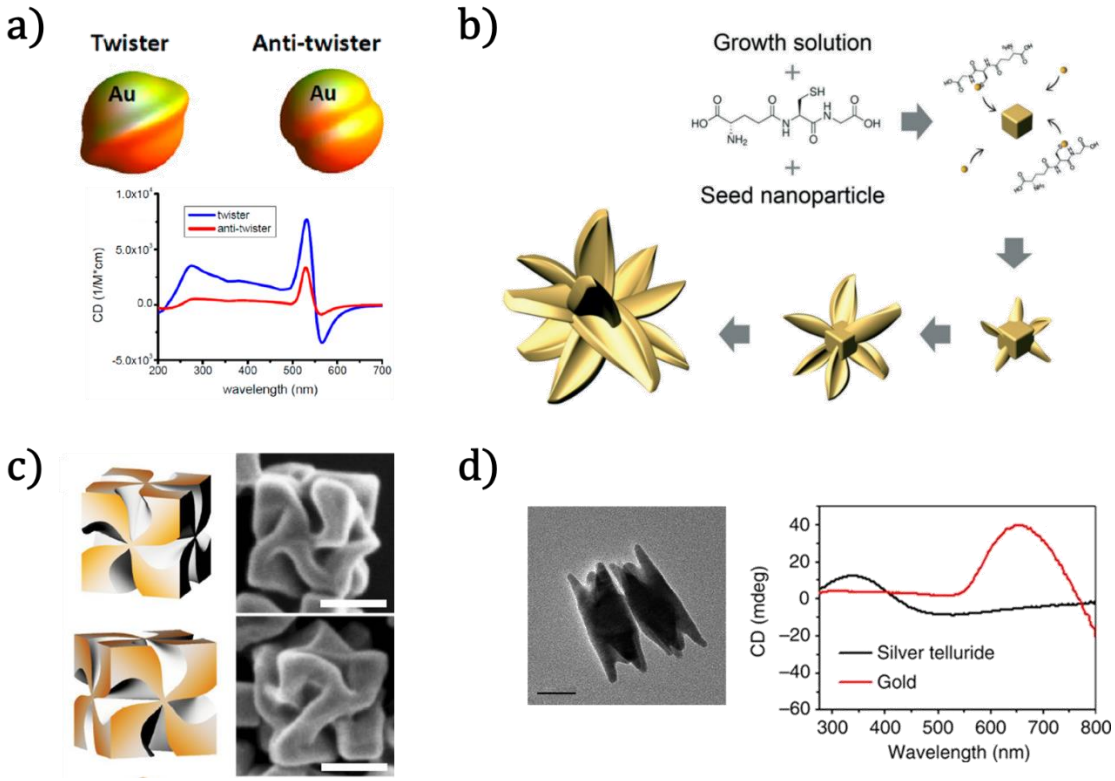

Figure 9. (a) Theoretical calculated CD signal of 'twister' and 'anti-twister' plasmonic crystals.[127] (b) Schematic illustration of the growth procedure of petal-like Au chiral structure.[184] (c) Plasmonic helicoid structure in different directions. (Scale bar 100 nm)[186] (d) TEM image of silver telluride chiral nanostructure. (Scale bar 200 nm, left) and CD spectra of gold and silver telluride nanostructure (right).[130] (a) Reproduced with permission.[127] Copyright 2012, American Chemical Society. (b) Reproduced with permission.[184] Copyright 2018, The Royal Society of Chemistry. (c) Reproduced with permission.[186] Copyright 2018, Springer Nature. (d) Reproduced with permission.[130] Copyright 2014, Springer Nature.

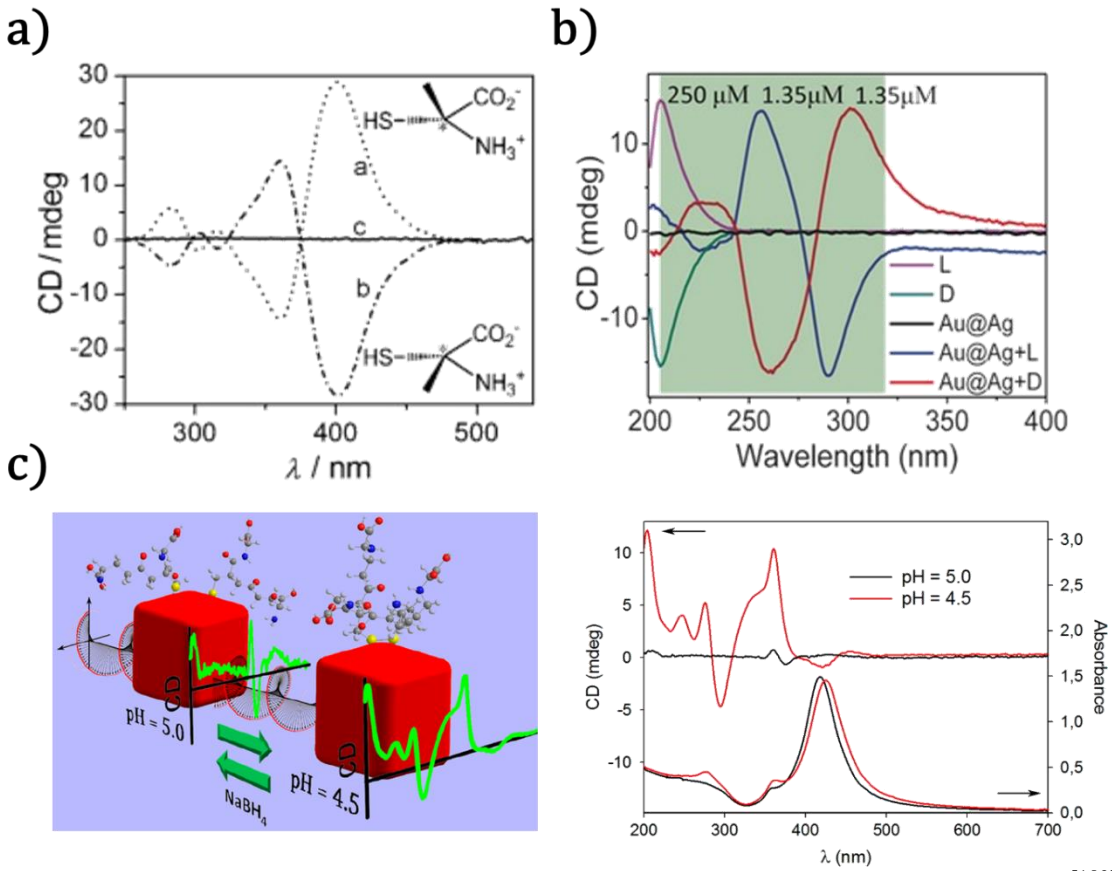

Figure 10. (a) CD spectra of Cys capped Ag NPs and Au@Ag core shell nanocuboids.[189] (b) CD spectra Au@Ag nanocuboids decorated with Cys.[63] (c) Schematic of pH regulated silver nanocubic-GSH conformation changes (left). Dialyzed cube-shaped Ag NPs complex at different pH value indicating the formation of diglutathione (right).[193] (a) Reproduced with permission.[189] Copyright 2012, Wiley. (b) Reproduced with permission.[63] Copyright 2017, Wiley. (c) Reproduced with permission.[193] Copyright 2015, American Chemical Society.

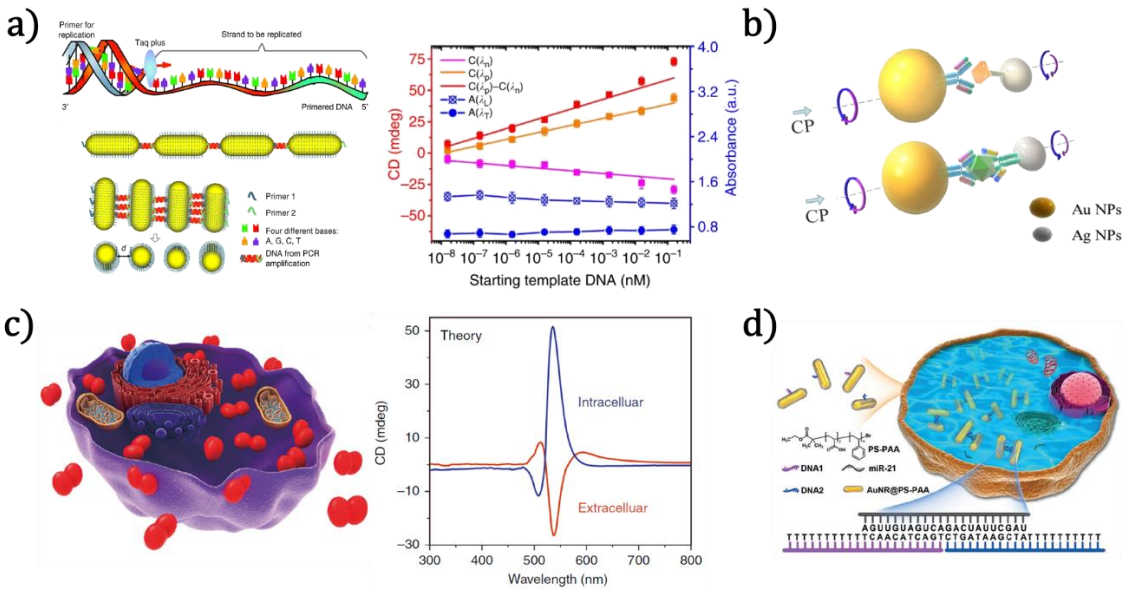

Figure 11. (a) Schematics of polymerase chain procedure based ETE and SBS assembly of Au NRs (left) and calibration curves obtained from CD and UV spectrum of SBS assemblies (right).[200] (b) Schematic illustration of the assembled Au-Ag heterodimer.[201] (c) Schematics of NP dimers inside a model cell (left) and the CD responses of intra/extracelluar Au NP dimers.[203] (d) Schematic representation of target miRNA formation of Au NR chiral SBS dimers.[204] (a) Reproduced with permission.[200] Copyright 2013, Springer Nature. (b) Reproduced with permission.[201] Copyright 2013, American Chemical Society. (c) Reproduced with permission.[203] Copyright 2017, Springer Nature. (d) Reproduced with permission.[204] Copyright 2013, Wiley.

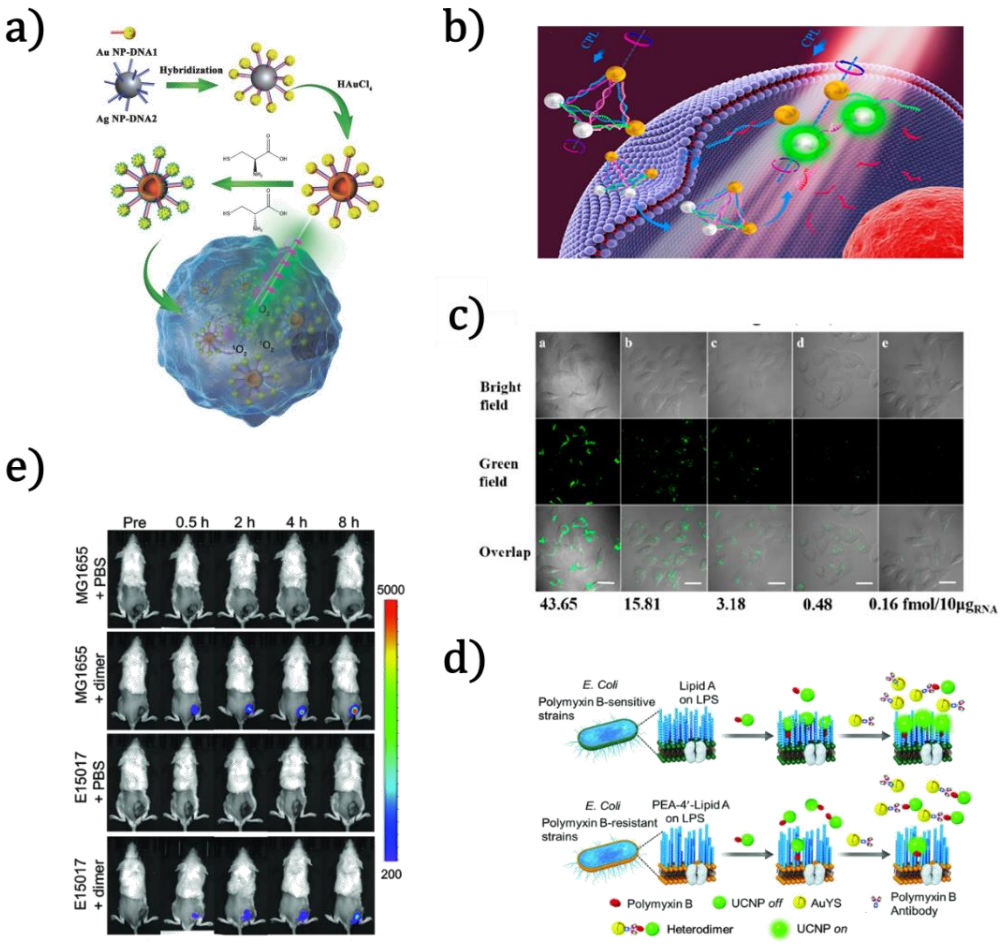

Figure 12. (a) Schematic illustration of AuYS and UCNP heterodimer for drug-resistant bacteria detection and imaging. (b) UCL imaging before and after i.v. injection of AuYS-UCNP heterodimer into inoculation of polymyxin-B-sensitive strains (MG1655), polymyxin-B-resistant bacteria (E15017) and PBS control. (c) Working principle of Au-UCNP for miRNA detection, Au-UCNP pyramids disassemble after arriving living cell (d) The schematic illustration of self-assembled shell-satellite nanostructure. (a) Reproduced with permission.[208] Copyright 2018, Wiley. (b) Reproduced with permission.[208] Copyright 2018, Wiley. (c) Reproduced with permission.[207] Copyright 2015, American Chemical Society. (d) Reproduced with permission.[206] Copyright 2017, Wiley.

Tables:

Mechanism	Configuration	Sensing Target	Limit of Detection	Ref.
Electromagnetic Interaction	Spherical Nanoparticle Dimer	Cysteine	20 pM	2013[198]
	Nanorod Assembly	Cu^{2+}	7 pM	2017[218]
	SBS nanorod	Hg^{2+}	0.03 ng / mL	2012[219]
	Core-shell	Zn^{2+}	3.87μM/10^6 cell	2018[113]
Chiral Assembly Chiral Assembly	Heterodimers	Ag^{+}	2 pM	2013[220]
	Prolate Nanoparticle Dimer	Telomerase Activity	$1.7x10^{-15}$ IU	2016[221]
	Heterodimers	prostate-specific antigen	15 zM	2013[201]
	SBS nanorod	DNA	3.7 aM	2013[200]
	SBS nanorod	miRNA	0.081 fmol / 10 μg_{RNA}	2018[204]
	DNA origami	aptamer	25μM	2018[196]
	DNA origami	RNA	100pM	2018[197]
	Heteropyramid	Hg^{2+}	0.2 pg/mL	2015[205]
	Heteropyramid	miRNA	0.03 fmol / 10 ug_{RNA}	2015[207]
Conformational Change	Core-shell	Cysteine	12.5 μM	2018[199]

Table 1: Summary of sensing mechanisms and their detection limits

Author Photographs and Biographies:

Zhaolong Cao is currently an Associate Professor at State Key Laboratory of Optoelectronic Materials and Technologies, Guangdong Province Key Laboratory of Display Material and Technology, and the School of Electronics and Information Technology, Sun Yat-Sen University. He received his BSc and PhD degrees all in Physics from University of Science and Technology of China and Chinese University of Hong Kong in 2010 and 2014, respectively. His current research interests are plasmonics, metamaterials, and optoelectronic devices in visible, infrared and terahertz frequencies.

Han Gao is current a PhD student in the Department of Electrical Engineering in the Hong Kong Polytechnic University. Her current research concentrates on the preparation and characterization of chiral inorganic assemblies and their applications in biological sensing and recognition.

Dangyuan Lei is currently an Associate Professor at the Department of Materials Science and Engineering in City University of Hong Kong. He received his BSc, MPhil and PhD degrees all in Physics from Northwest University, Chinese University of Hong Kong and Imperial College London in 2005, 2007 and 2011, respectively. His research interest centres on nanophotonics and optical spectroscopies, with particular interest in plasmon-enhanced light-matter interaction at the nanoscale and its applications in energy harvesting, biosensing, and bioimaging.